LA-UR-15-22858
Approved for public release; distribution is unlimited.

Title: Field Evaluation of the Restorative Capacity of the Aquifer Downgradient of a Uranium In-Situ Recovery Mining Site

Author(s): Reimus, Paul William

Intended for: Report

Issued: 2015-05-22 (rev.1)

Field Evaluation of the Restorative Capacity of the Aquifer Downgradient of a Uranium In-Situ Recovery Mining Site

Paul Reimus[1], Michael Rearick[1], George Perkins[1], Oana Marina[1],
Jesse Punsal[1], Naomi Wasserman[2], Kevin Chamberlain[3] and James Clay[4]

[1]Los Alamos National Laboratory
[2]Los Alamos National Laboratory, currently University of Illinois at Urbana-Champaign
[3]University of Wyoming
[4]Cameco Resources

Executive Summary

A two-part field study was conducted to evaluate the restorative capacity of the aquifer downgradient (i.e., hydrologically downstream) of a Uranium in-situ recovery (ISR) mining site with respect to the transport of uranium and other potential contaminants in groundwater after mining has ceased. The study was conducted at the Smith Ranch-Highland ISR facility near Douglas, WY, operated by Cameco Resources. Because it was not possible to conduct field experiments involving elevated concentrations of uranium or other potential contaminants in an aquifer downgradient of an ore zone (by definition this would constitute an 'excursion' requiring corrective action), the tests were conducted in ore zone wells in two different mining units.

The first part of the study involved conducting cross-well tracer tests in two five-spot well patterns in Smith Ranch mining unit 4 (MU-4), which was mined by ISR from 1999 to 2005 and is currently in the process of being restored by groundwater sweep and reverse osmosis treatment. The tracer tests were conducted to evaluate hydrologic sweep in the two five-spot patterns, which was then used to predict the hydrologic dispersion of a residual contaminant 'plume' as it migrates from an ore zone into the aquifer downgradient of an ore zone. It was assumed that the flow heterogeneity in the two patterns was representative of the flow heterogeneity existing downgradient of an ore zone. The results of the tests indicated that the flow heterogeneity in the aquifer is not extreme and that dispersion downgradient of the ore zone can be represented using a Peclet number (travel distance divided by longitudinal dispersivity) of about 8. The results of the cross-well tracer tests were also useful for the planning of a pilot bioremediation field test that was subsequently conducted in one of the two five-spot patterns by the University of Wyoming in collaboration with Cameco Resources.

The second part of the study involved injecting waters withdrawn from two different wells in MU-4A (previously mined) at Smith Ranch into three different wells in the ore zone of MU-7 (unmined), and then pumping the wells back after allowing the injected waters to sit in the ore zone for different periods of time. These tests are referred to as 'push-pull' tests. The two MU-4A wells differed in that one had not undergone any restoration and its water had a uranium concentration of about 40 mg/L and an alkalinity of about 550 mg/L $CaCO_3$, while the other had undergone groundwater sweep and reverse osmosis treatment and its water had a uranium concentration of about 5 mg/L and an alkalinity of about 275 mg/L $CaCO_3$. The water from the unrestored MU-4A well was injected into two different MU-7 wells, and 'wait periods' of approximately 2 weeks and 3 months, respectively, were implemented before the wells were pumped back. The water from the partially-restored MU-4A well was injected into a third MU-7 well and allowed to sit for approximately 3 months before being pumped back. All of the injected

LA-UR-15-22858

waters were spiked with non-reactive tracers so that the return of the injected water could compared to the return of uranium and other constituents in the injected water. It was assumed that the geochemical conditions in the unmined ore zone were representative of the geochemical conditions downgradient of the ore zone. Available data suggest that this is a reasonable assumption.

The push-pull tests indicated that uranium from the MU-4A waters was strongly attenuated in the ore zone aquifer, with only 13-23% of the uranium being recovered when the MU-7 wells were pumped back and the uranium concentrations declining to near background levels before pumping ceased in all three wells. Recoveries of the nonreactive tracers suggested high recoveries of the injected waters in all the wells. Uranium isotope analyses indicated that there was not a significant shift in ^{238}U to ^{235}U ratios in the water pumped back from the push-pull tests, which suggests that biotic reduction (from U(VI) to U(IV)) was not a significant uranium attenuation process. However, uranium reduction by abiotic processes cannot be ruled out. ^{234}U to ^{238}U ratios were used to distinguish between injected uranium and uranium mobilized from the ore zone during the tests, and a significant amount of mobilized uranium was observed in all three push-pull tests. Other constituents, such as vanadium and selenium, were also clearly mobilized during the push-pull tests, which precluded an evaluation of the ability of the downgradient aquifer to attenuate the transport of these constituents.

A non-mechanistic multi-site, multi-rate adsorption/desorption transport model was used to interpret that uranium concentration-vs.-time histories in each of the push-pull tests, and the resulting model parameters were used to predict uranium transport in the aquifer downgradient of an ore zone over much longer time and distance scales than were interrogated in the tests. A conservative approach was taken in which it was assumed that there was only reversible adsorption of uranium and no irreversible attenuation (i.e., reduction) of uranium. The dispersion parameters deduced from the cross-well tracer tests were used in the predictive model. The results of the modeling indicate that the downgradient aquifer should significantly attenuate the transport of uranium, even without taking credit for any irreversible uranium immobilization, and if uranium reduction or some other irreversible immobilization process occurs, the attenuation should only be greater than predicted.

Introduction

Background and Study Objectives

The in-situ recovery (ISR) of uranium involves the injection, via an array of wells, of O_2- and CO_2- (or $NaHCO_3$-) fortified water (i.e., lixiviant) into a uranium-bearing ore zone to oxidize and solubilize the uranium (Pelizza, 2008). The solubilized uranium is pumped to the surface, where it is extracted and processed into uranium oxide (yellowcake). The water is then re-fortified with O_2 and CO_2 and used to recover more uranium. The process works best in roll-front uranium deposits that are below the water table and lie between aquitards that confine the injected lixiviant to the ore zone. ISR now accounts for most of the uranium produced in the U.S., and about half of the uranium produced worldwide (World Nuclear Association, 2014). The process avoids the extraction and processing of solid ores and does not leave behind underground mine workings or pits, nor tailings piles. However, ISR does significantly alter the geochemistry of ore zones, and it leaves behind elevated concentrations of uranium, as well as many other metals and potential contaminants, in ore zone groundwaters. The industry practice is to reduce the concentrations of these constituents after mining by a combination of drawing groundwater in from outside the ore zone to replace the existing groundwater (groundwater sweep), treatment of the groundwater by reverse osmosis to remove total dissolved solids, and the use of chemical reductants to reverse oxidation of aquifer waters and sediments. These practices work well to significantly reduce constituent concentrations, but they typically do not succeed in lowering concentrations of all species to pre-mining 'baseline' levels, particularly over extended periods of time.

The industry and its regulators (EPA, NRC, and state agencies) are currently working toward an ISR regulatory framework that considers best mining and restoration practices, restoration and monitoring costs, the need to protect groundwater resources, the realities of geochemical changes resulting from ISR mining, and relative risks to the environment and the public. This study is intended to inform this effort, and in particular, to suggest and demonstrate an approach to evaluating the ability of the aquifer downgradient of uranium ore zones to attenuate the transport of uranium and other potential problem constituents to accessible groundwater supplies. By 'downgradient' we mean here the portion of the aquifer into which water from an ore zone flows; i.e., hydrologically downstream of the ore zone. If such attenuation can be better estimated and quantified, then it might be possible to relax conservatism in ore zone restoration targets and in post-restoration monitoring requirements while still ensuring the safety of the environment and the public.

Study Site

The study was conducted at the Smith Ranch-Highland ISR facility near Douglas, WY, operated by Cameco Resources. Fig. 1 shows a map of the site, including the two areas where the field tests were conducted. The site hosts multiple roll-front uranium deposits that are in various stages of exploration, ISR mining, or restoration and stability. Smith Ranch-Highland is the largest uranium ISR operation in the U.S., accounting for approximately 1/3 of all domestic uranium production in recent years.

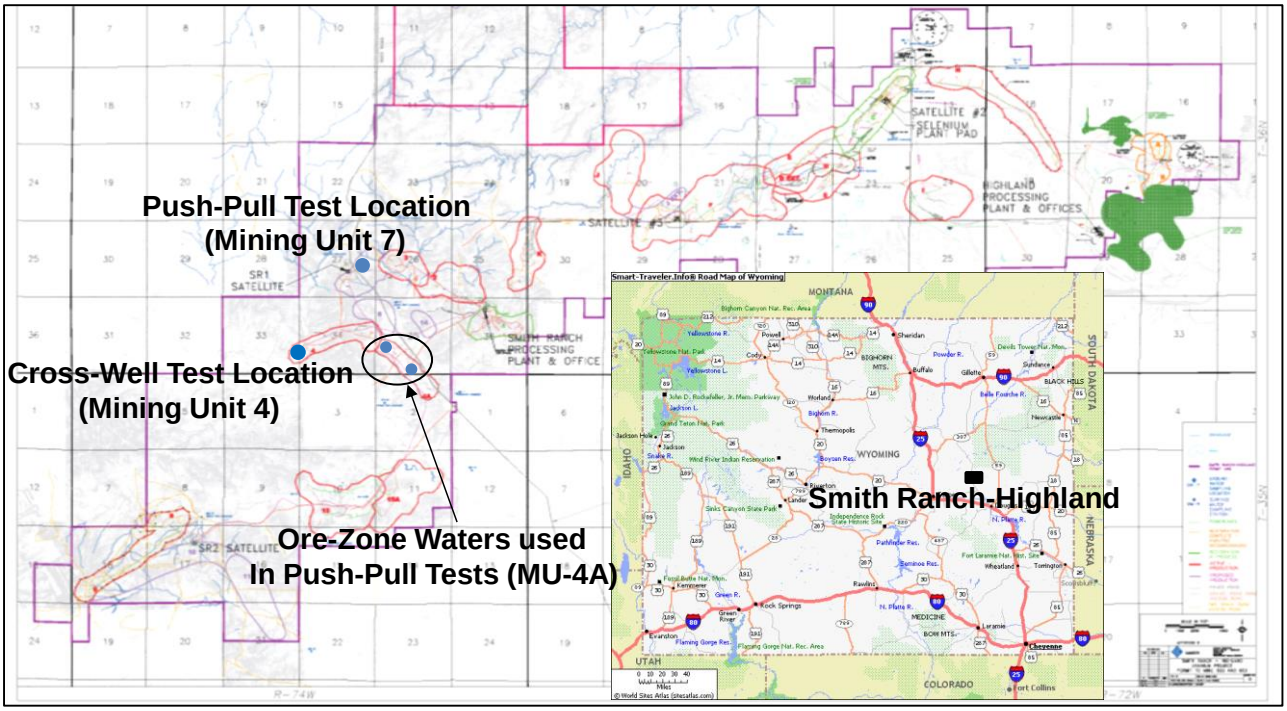

Figure 1. Map showing location of Smith Ranch-Highland operation and locations of the field tests conducted for this study. Irregular-shaped regions are mining units in various stages of exploration, operation, restoration or stability.

Field Test Methods and Conduct

The field study consisted of two parts: (1) a pair of cross-well tracer tests in an aquifer hosting a uranium ore body, and (2) three single-well push-pull tests in which water from a previously-mined ore zone was injected into and then withdrawn from an unmined ore zone. Both sets of tests were conducted using existing wellfield infrastructure designed for uranium extraction; the cross-well tests were conducted in mining unit 4 (MU-4), which was mined from 1999 to 2005 and is currently in restoration by groundwater sweep and reverse osmosis treatment, and the push-pull tests were conducted in an area of MU-7 that had not yet been mined. For the purposes of this study, it would have been more desirable to conduct the tests downgradient of ore zones, but downgradient wells in the proper configuration for cross-well testing were not available, and the injection of water from a previously-mined ore zone into downgradient wells would, by definition, have resulted in an 'excursion' of lixiviant from the ore zone that would have required corrective action. An implicit assumption in this study was that the hydrology and, in the case of the push-pull tests, geochemistry of the ore zones in which the tests were conducted were representative of the aquifers downgradient of the ore zones. The geochemical similarity of an unmined ore zone to a downgradient aquifer seems reasonable at Smith Ranch given that roll-front uranium deposits formed at redox boundaries where oxidizing waters encountered geochemically reducing conditions, and the fact that the uranium remained in place implies that the conditions within and downgradient of the ore zone remained reducing. Furthermore, core taken from within and downgradient of an ore zone in MU-3, located near MU-7, was very similar in appearance and mineralogy, and water quality data from these coreholes were also generally very similar.

Cross-Well Tracer Tests

The cross-well tracer tests were intended to interrogate the flow heterogeneity in the aquifer so that this information could be used to help predict the downgradient transport of contaminants. 'Flow heterogeneity' here refers to the non-uniform distribution of flow within an aquifer that leads to spreading or 'smearing' of a contaminant plume and ultimately results in some early arrival of contaminant at a compliance point relative to the mean contaminant arrival time. This spreading can also be beneficial in that some contaminant mass will arrive later than the mean arrival time, with the net result being a lowering of the peak contaminant concentration observed at the compliance point.

The tests were conducted in two five-spot well patterns that were served by header house 4-6 (HH 4-6) in MU-4. A header house is a small building into which a contiguous block of injection and extraction wells from a mining unit are plumbed for access at the surface. During mining, the flows from all the production wells in a header house are combined and sent to a processing plant for uranium extraction by ion exchange, and all the injection wells are fed by a single 'header' that supplies O_2- and CO_2-fortified water to the ore zone. The two five-spot test patterns were spatially separated by enough distance that it was considered very unlikely that there would be interference between the two tests. Fig. 2 shows the locations of the two test patterns within the block of wells served by HH 4-6. Each roughly square-shaped pattern had a production well at the center and an injection well at each of the four corners. Fig. 3 shows the layouts of the two patterns, including the length of the well screens in each well and the distance between each injection well and the central production well. The depth to the ore zone in each pattern was approximately 750 to 780 feet below land surface. The tracer tests were started in late September 2013, and they were completed in mid-November 2013.

The tests were conducted by first modifying the plumbing in the header house to isolate the two patterns and then establishing steady circulating flow within each pattern, with the water from the production well being distributed approximately equally into the four injection wells in the patterns. There was no hydrologic 'bleed' (i.e., diversion of a fraction of the production flow resulting in a net withdrawal of water) from the patterns. After steady flow was established, nonreactive tracers were injected sequentially into each of the four injection wells at a rate that insignificantly affected the overall flow rates into the wells. The tracers used were 2,6-difluorobenzoate, 2,5-difluorobenzoate, 2,4-difluorobenzoate, and pentafluorobenzoate, all of which were injected as sodium salts. The principal investigator has considerable experience using fluorinated benzoates as nonreactive groundwater tracers, and these tracers also have widespread acceptance within the groundwater tracing scientific community. 5 kg of a different fluorinated benzoate salt was injected into each corner well in each pattern so that the response from each injector could be distinguished from the other injectors. The fluorinated benzoates injected into each well are indicated in Fig. 3. 1.5 kg of sodium iodide was also injected into each of the four corner injection wells in each pattern. The sodium iodide was used primarily to serve as a field indicator of when tracers arrived at the production wells, as iodide is also a nonreactive tracer and it can be easily and quickly measured using an ion-selective electrode (the fluorinated benzoates require a more complex analytical procedure that was not possible to implement at the Smith Ranch-Highland facility). The time periods of tracer injection into each well were staggered and varied in duration because of logistical constraints and some equipment problems; these time periods are listed in Table 1. The arrivals of iodide at the production wells were used to help guide sampling frequencies at these wells early in the tests to ensure that the tracer breakthroughs were adequately captured. Two ISCO Foxy 200 autosamplers were fed by a low-flow sidestream

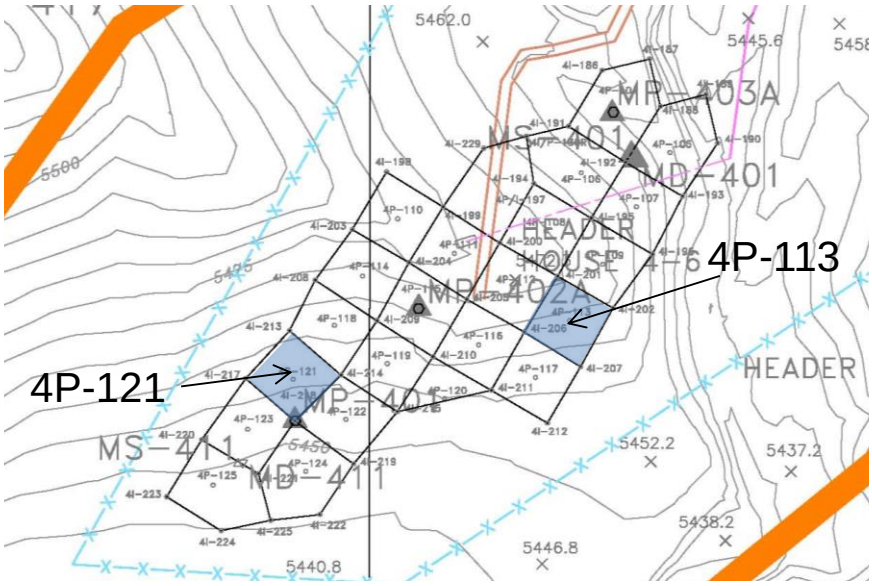

Figure 2. Locations of the two well patterns within the block of wells served by HH 4-6 that were used for cross-well tracer tests. Production wells are at the centers of each polygon and injection wells are at the corners of each polygon. Each square is about 100' on a side.

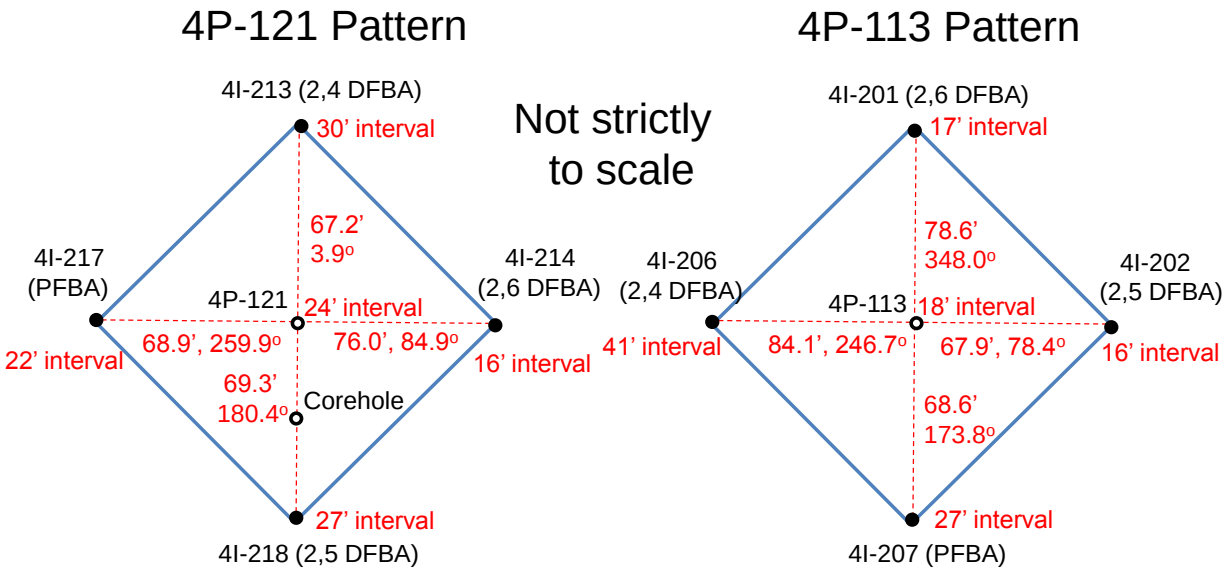

Figure 3. Details of the two well patterns used for cross-well tracer testing. Lengths are in feet. Angles are azimuths relative to the production well, with 0/360° being true north. Fluorinated benzoates (FBAs) injected into each corner well are indicated in parentheses.

diverted from the main production flows in each pattern to continuously collect water samples throughout the tests. Appendix A includes some photos showing the test setup within HH 4-6.

The fluorinated benzoates and iodide concentrations in the groundwater samples were quantified by high-performance liquid chromatography (HPLC) at Los Alamos National Laboratory using a Dionex Ultimate 3000 RS Variable Wave Length Detector. The primary analytical column was an Acclaim C-18 (4.6 x 150 mm). Typical analytical parameters were as

Table 1. Injection times for each of the cross-well tracer test injections.

Injection Well/Tracer	Start Date/Time	End Date/Time	Comments
4I-214 / 2,6 DFBA+I^-	9/26/13 17:05	9/27/13 11:10	
4I-201 / 2,6 DFBA+I^-	9/26/13 17:05	9/27/13 11:10	
4I-213 / 2,4 DFBA+I^-	9/27/13 17:32	9/28/13 16:13	
4I-206 / 2,4 DFBA+I^-	9/27/13 17:32	9/28/13 16:23	
4I-217 / PFBA+I^-	9/28/13 16:50	9/29/13 12:23	
4I-207 / PFBA+I^-	9/28/13 16:50	9/29/13 12:42	
4I-218 / 2,5 DFBA+I^-	9/29/13 13:24	9/30/13 11:58	Injection interrupted 9/30 ~4:30 and resumed 9/30 @ 7:40
4I-202 / 2,5 DFBA+I^-	9/29/13 13:24	9/30/13 22:16	Injection interrupted 9/29 ~15:30 due to pump failure and resumed 9/30 @ 12:11

follows: 60/40 v/v 30 mM KH_2PO_4 buffer/methanol; 25°C; 0.8 mL/min flow rate; 200 µL injection volume; and analyte detection at 222 nm.

Fig. 4 shows the flow rates recorded in each of the injection wells and the production wells of the two patterns during the approximately six-week period of the cross-well tests. Differences between the sum of the injection flows and the production flows are attributed to flow measurement errors, as all of the production flows were routed to the injectors. The flows within the patterns were reasonably well balanced throughout the tests, although there were minor fluctuations and periods of slight imbalance between the injectors. There were two significant periods of weather-related power outages that resulted in flow stoppages during the tests, indicated in Fig. 4. These flow stoppages did not compromise the tests, as the ambient flow in the aquifer during these short time periods should have caused very little movement of tracers relative to their movement under the influence of the circulating flows. When plotting the tracer breakthrough curves and interpreting the test results, the tracer concentrations were taken to be a function of volume of water produced rather than time to avoid having to account for the flow stoppages.

Although it really didn't matter for the tracer tests, the two test patterns had recently been restored by groundwater sweep and reverse osmosis treatment, so the waters within the patterns had relatively low uranium concentrations (on the order of 1 mg/L). One of the patterns (centered on 4P-121) was subsequently used for a bioremediation pilot test, and the tracer test results helped with the planning of this test.

Single-Well Push-Pull Tests

The single-well push-pull tests were intended to interrogate the ability of the downgradient aquifer to attenuate the transport of uranium and other potential problematic constituents as ore zone water flows downgradient. It is expected that uranium and other problem constituents such as selenium and radium will be attenuated by a combination of adsorption onto aquifer solids and, for redox-sensitive species like uranium and selenium, reduction and subsequent precipitation of the less-soluble reduced species. The latter process is likely to be more permanently immobilizing, as the geochemical conditions outside mined ore zones at Smith Ranch-Highland are quite reducing, and it thus seems unlikely that immobilized reduced species would be

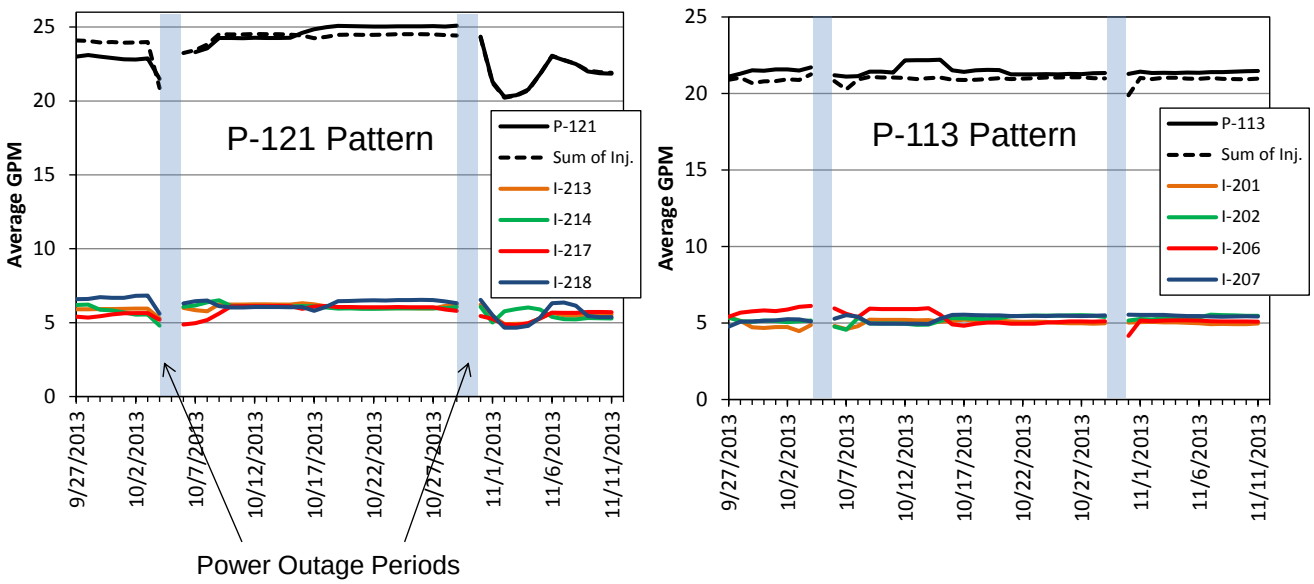

Figure 4. Injection and production flow rates during the two cross-well tracer tests.

re-oxidized and re-mobilized. The information from the push-pull tests was coupled with the flow heterogeneity information from the cross-well tracer tests to predict downgradient transport. However, as will be shown, the push-pull tests yielded information only on the attenuation of uranium, not selenium or any other elements, so the predictions are limited to uranium transport downgradient of the ore zone.

The push-pull tests were conducted by injecting waters withdrawn from two different wells in MU-4A (previously mined) into three different wells in the ore zone of MU-7, and then the wells were pumped back after allowing the injected waters to sit in the ore zone for different periods of time. The MU-7 wells were accessed in Header House 7-5, which had not yet gone into production, so the wells were in a portion of the MU-7 ore zone that had not yet been exposed to O_2 and CO_2 and was thus was considered to have geochemical conditions that were reasonably representative of the geochemical conditions in the downgradient aquifer. The relative locations of the MU-7 wells used in the push-pull tests are shown in Fig. 5. The two MU-4A wells were 4P-61 and MP-423, and the general water chemistry data for these wells are listed in Table 2, which also lists the water chemistry data for the chase water well, 7P-38. 4P-61 was undergoing groundwater sweep and reverse osmosis treatment at the time of the push-pull tests, and its water had a uranium concentration of about 4.7 mg/L, with an alkalinity of about 275 mg/L $CaCO_3$. MP-423 had not undergone any restoration and its water had a uranium concentration of about 40 mg/L, with an alkalinity of about 550 mg/L $CaCO_3$. Thus, the push-pull tests featured a partially-restored groundwater and an unrestored groundwater that effectively served as a worst-case scenario.

Table 3 provides the solution speciation of uranium in the two injection waters as calculated using the geochemical code PHREEQC (Parkhurst and Appelo, 2013) with the Lawrence Livermore National Laboratory geochemical databaste (Johnson, 2010) supplemented with complexation constants reported by Dong and Brooks (2006) for ternary uranyl-Ca/Mg-carbonate complexes. It is apparent that in both waters uranyl-Ca-carbonate complexes dominate the uranium speciation. However, it is noteworthy that despite the factor of 8-9 lower total

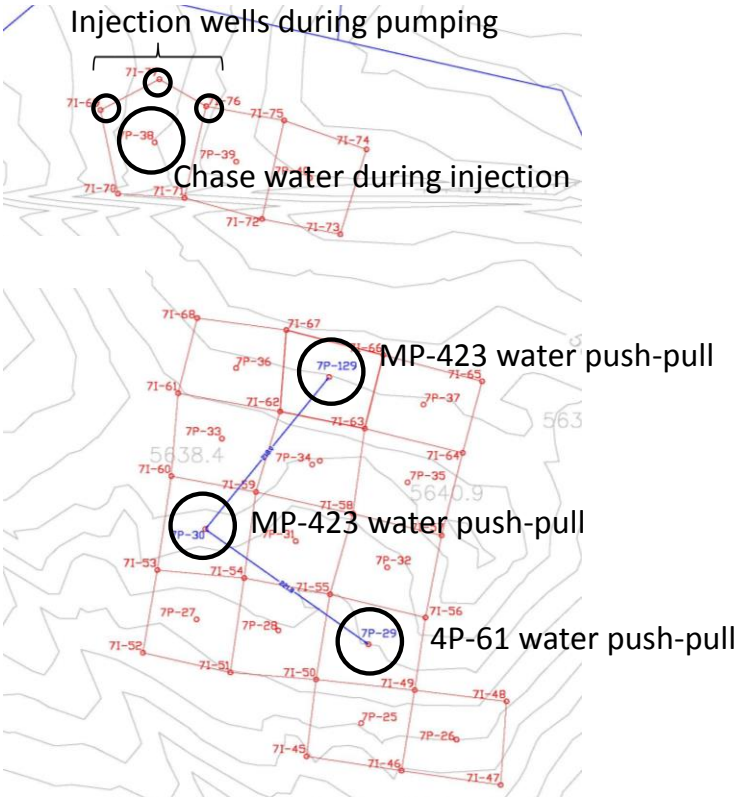

Figure 5. Locations of the wells used in the push-pull tests (all served by HH 7-5). The three circled wells in the bottom set of patterns were the push-pull wells (7P-129, 7P-30, and 7P-29, from top to bottom). The large circle in the upper set of patterns indicates the well pumped for chase water, and the three smaller circles indicate the wells used for injection of water pumped from the push-pull wells. Each square pattern is approximately 100' on a side.

Table 2. Major chemistry of the MP-423 and 4P-61 well waters used for push-pull injections and the 7P-38 well water used as chase water in the push-pull tests.

Constituent	MP-423	4P-61	7P-38
Ca^{2+} (mg/L)	461	162	102
Na^{+} (mg/L)	46	28	26
Mg^{2+} (mg/L)	108	42	26
K^{+} (mg/L)	20	12	8
Fe (total, mg/L)	2.5	2.0	0.3
Uranium (mg/L)	40.7	4.7	0.17
Si (mg/L)	7.5	6.5	7.5
SO_4^{2-} (mg/L)	895	300	290
Cl^{-} (mg/L)	131	41	2.2
Alkalinity (mg/L as $CaCO_3$)	550	275	160
HCO_3^{-} (mg/L calculated)	670	335	195
pH	~6.3	~6.3	~7.4

Table 3. Uranium speciation in MP-423 and 4P-61 waters as calculated using PHREEQC.

Uranium Species	MP-423, M	MP-423 Fraction	4P-61, M	4P-61 Fraction
$Ca_2UO_2(CO_3)_3^0$	1.53×10^{-4}	0.8900	1.61×10^{-5}	0.8140
$CaUO_2(CO_3)_3^{-2}$	1.78×10^{-5}	0.1040	3.38×10^{-6}	0.1709
$MgUO_2(CO_3)_3^{-2}$	6.21×10^{-7}	0.0036	1.26×10^{-7}	0.0064
$UO_2(CO_3)_2^{-2}$	1.33×10^{-7}	7.77×10^{-4}	9.49×10^{-8}	0.0048
$UO_2(CO_3)_3^{-4}$	1.31×10^{-7}	7.62×10^{-4}	2.90×10^{-8}	0.0015
$Mg_2UO_2(CO_3)_3^0$	1.17×10^{-7}	6.83×10^{-4}	1.41×10^{-8}	7.12×10^{-4}
UO_2CO_3	2.05×10^{-8}	1.19×10^{-4}	3.05×10^{-8}	0.0015
$SrUO_2(CO_3)_3^{-2}$	8.80×10^{-9}	5.14×10^{-5}	2.34×10^{-9}	1.18×10^{-4}
$UO_2(OH)_2$	6.76×10^{-10}	3.94×10^{-6}	1.68×10^{-9}	8.50×10^{-5}
UO_2OH^+	4.70×10^{-11}	2.74×10^{-7}	1.11×10^{-10}	5.60×10^{-6}
$(UO_2)_2CO_3(OH)_3^-$	1.09×10^{-11}	6.37×10^{-8}	3.81×10^{-11}	1.93×10^{-6}
UO_2^{+2}	7.17×10^{-12}	4.18×10^{-8}	1.43×10^{-11}	7.25×10^{-7}

uranium concentration in the 4P-61 water relative to the MP-423 water, the concentration of uncomplexed uranyl ion (UO_2^{2+}), which is the solution species that is typically assumed to participate in surface adsorption reactions (Davis and Curtis, 2003), is predicted to be greater in the 4P-61 water than in the MP-423 water. Thus, based on these geochemical calculations and conventional thinking about uranyl ion being the reactive species at mineral surfaces, the uranium in the 4P-61 water would be expected to be more reactive than uranium in the MP-423 water. This result is consistent with the expectation that it should be easier to immobilize uranium from a restored or partially-restored water than from an unrestored water.

Approximately 1500 gallons of water from 4P-61 was injected into well 7P-29 on September 30, 2014, and this water was then 'chased' with approximately 6000 gallons of water from well 7P-38. Prior to injection, the 4P-61 water was transported in a tank truck from 4P-61 to HH 7-5, and the head space in the truck was purged with a pressurized gas mixture that was 4% H_2, 4% CO_2, and balance N_2 in an attempt to limit the introduction of O_2 into the water and keep the water relatively reducing while not significantly degassing CO_2. The headspace was reduced to about 2% O_2 (from atmospheric starting conditions) during the gas purge. Approximately 1500 gallons and 1100 gallons of water from MP-423 were similarly injected into wells 7P-30 and 7P-129 on October 1 and 2, 2014, respectively, and these injections were followed immediately with approximately 5000 and 4700 gallons, respectively, of water from well 7P-38. The O_2 levels in the headspace of the tank truck for the latter two injections were slightly higher than in the 7P-29 injection because less gas was used for the headspace purges. Table 4 summarizes the injection and chase volumes used in each well, and also the volumes eventually pumped from the wells, which are discussed below. Also included in Table 4 are the lengths of the wellscreens in the three MU-7 push-pull wells and estimates of how far into the aquifer the injected waters would have been pushed if flow were ideally radial and confined (assuming a flow porosity of 0.25).

7P-38 was chosen as the chase water well because of its spatial distance from the injection wells (Fig. 5) so that when it was pumped it would not draw the tracers away from the injection wells. The 7P-38 water chemistry is listed in Table 2 and was considered to be representative of the groundwater in the unmined areas of MU-7. The background concentration of uranium in the unmined MU-7 ore zone water was considered low enough relative to the concentrations in the MU-4A waters that it was expected to be easy to see the elevation of uranium in the waters

Table 4. Injection, chase and pumped volumes used in push-pull tests and calculated penetration distances into the aquifer of injection solutions under ideal radial flow conditions.

Quantity	7P-129	7P-30	7P-29
Injection (4P-61/MP-423), gallons	1100	1520	1550
Chase (7P-38), gallons	4680	5060	5900
Pumped, gallons	24,500	90,000	61,000
Wellscreen length, ft	16	19	24
Penetration distance, ft	8.8	8.5	8.2

resulting from the high concentrations in the MU-4A waters when the wells were pumped back. The 'chase' water was injected to ensure that the MU-4A waters were 'pushed' out into the formation away from the injection wellbores so that they would experience contact only with the solids in the ore zone and not linger in the wells. 1.5 kg of sodium 2,6-difluorobenzoate, 1.5 kg of sodium bromide, and 1.5 kg of sodium iodide were added to each of the MU-4A waters to serve as nonreactive tracers that would allow the recovery of these injected waters to be monitored when the MU-7 wells were pumped back and, more importantly, to allow comparison of the recovery of these tracers with the recoveries of uranium and other constituents so that the attenuation of these constituents in the aquifer could be quantified.

Well 7P-129 was pumped back starting on October 21, 2014, and approximately 25,000 gallons were produced over a 3-day period. The pumping rate was approximately 9 gpm. Two autosamplers were set up to collect water from the production flow stream at regular intervals; one was loaded with glass bottles for tracer analyses, and the other with plastic bottles for analyses of anions, cations, and trace elements. Photos of the collection system are included in Appendix B. The production flow was routed into injection wells 7I-69, 7I-76 and 7I-77, which are located near 7P-38 and are spatially distant from the injection wells to avoid pushing tracers away from the injection wells.

Wells 7P-30 and 7P-29 were pumped back starting on January 7 and January 10, 2015, respectively. The initial pumping rate in both wells was approximately 9 gpm, but the rate was increased to about 27-28 gpm in both wells during the tests to speed the recovery of tracers. Approximately 90,000 gallons was produced from 7P-30 and slightly more than 60,000 gallons was produced from 7P-29. The autosamplers were again used for sample collection, and the same three injection wells (7I-69, 7I-76 and 7I-77) were used to accept the water produced from 7P-30 and 7P-29. After all pumping was completed, well 7P-38 was sampled to see if any of the tracers injected into 7I-69, 7I-76 and 7I-77 had made it to 7P-38, but tracers were not detected in the 7P-38 water.

During pumping of the three wells used for the push-pull tests, a YSI 650XLM sonde and meter system were used to continuously log, at 1- to 2-minute intervals, the temperature, pH, oxidation-reduction potential (ORP), and specific conductance of a portion of the production flow that was routed through a flow cell. Photos of the deployed system are included in Appendix B. The pH probe was calibrated using pH 4, 7, and 10 standard buffer solutions (Thermo-Fisher Scientific and GeoTech), the specific conductance probe was calibrated using a 1413 μS/cm KCl standard solution (GeoTech), and the ORP probe was calibrated using the pH 4 and 7 buffers that were saturated with quinhydrone (prepared fresh each time) to produce solutions of known ORP at a given temperature. The temperature probe was not calibrated but was checked periodically by comparing to standard thermometers and was found to be within 1°C agreement. Calibrations

were repeated multiple times during each test, and the drift for each probe was quite low (within 0.1 unit for pH, within 10-15 uS/cm for specific conductance, and within 10 mV for ORP – often no recalibration was deemed necessary).

In addition to the continuously logged YSI parameters, the alkalinity of the produced waters were periodically measured using a Hach digital titrator and titration with H_2SO_4 to a bromocresol green-methyl red indicator endpoint (Hach Method 8203). Also, Hach reagent kits were used for periodic measurements of ferrous iron and sulfide concentrations in the waters using Hach Methods 8146 and 8131, respectively (www.hach.com). The ferrous iron and sulfide measurements indicated relatively low concentrations of both constituents and did not show any significant trends in the produced waters, so they are not reported here.

The YSI sonde/meter and the Hach kits were also used to measure the parameters mentioned above in each of the injection waters and in the 7P-38 chase water during the injections into the MU-7 wells.

Grab samples were also collected during each of the push-pull injections and periodically during each of the pumping periods for uranium isotope analyses at the University of Wyoming, Geology and Geophysics Dept. These samples were filtered through a 0.45-μm cartridge filter directly into 125-ml high-density polyethylene bottles certified for low metals content, and then they were immediately acidified using approximately ~1 ml of ultra-trace-metal-pure HNO_3 (Optima). The samples were delivered to the University of Wyoming within a week of collection.

The 2,6 difluorobenzoate and iodide concentrations were measured in the test samples using the same HPLC method that was used for these tracers in the cross-well tracer tests (see above). Anions (other than HCO_3^-), including the tracer bromide, were analyzed at Los Alamos National Laboratory by ion chromatography using EPA method 300 on the Dionex DX-600 system. Major cations were analyzed at Los Alamos by inductively coupled plasma-optical emission spectroscopy (ICP-OES) using EPA Method 200.7 on a Perkin Elmer Optima 2100 DV. Ultra high-purity nitric acid (Fisher Trace Metal Grade) was used in sample and calibration preparation prior to sample analysis. An internal standard (Sc) was added to both samples and standards to correct for matrix effects, which can result in varying sample introduction rates. Some samples were diluted prior to analysis to minimize matrix effects as well as allow the analytes of interest to remain within the linear dynamic range of the calibration. SPEX CertiPrep Instrument Check Standard 3 was used to check the accuracy of the multi-element calibrations. Typical ICP-OES parameters were: 1350 W forward power, 15 L/min plasma gas flow, 0.2 L/min auxiliary flow; and 0.8 L/min nebulizer flow.

Minor elements, including uranium, selenium, vanadium and arsenic were analyzed at Los Alamos by inductively coupled plasma-mass spectrometry (ICP-MS) using EPA method 200.8 on a Perkin Elmer NexION system. As with the ICP-OES samples, ultra high-purity nitric acid (Fisher Trace Metal Grade) was used in sample and calibration preparation prior to sample analysis. Internal standards (Y, Bi, and In) were added to both samples and standards to correct for matrix effects which can result in varying sample introduction rates. Some samples were diluted prior to analysis to minimize matrix effects as well as allow the analytes of interest to remain within the linear dynamic range of the calibration. Standard Reference Material (SRM) 1640a Trace Elements in Natural Water was used to check the accuracy of the multi-element calibrations. Typical ICP-MS parameters were: 1600 W forward power, 18 L/min plasma gas flow, 1.2 L/min auxiliary flow; and 0.9 L/min nebulizer flow. Chromium, Selenium, and Arsenic were analyzed using Kinetic Energy Disciminator (KED) mode to diminish isobaric interferences.

In addition to the measurements conducted at Los Alamos, numerous grab samples collected during the pumping of each MU-7 well were analyzed for uranium by ICP-OES at the Smith Ranch-Highland facility. Although these data are not reported here, they were in excellent agreement with the Los Alamos ICP-MS uranium results, and they provided quick-turnaround uranium concentration measurements that were invaluable for determining when each well had been pumped sufficiently to have reached close to background uranium concentrations and thus when each test could be terminated.

$^{234}U/^{238}U$ ratios and $^{238}U/^{235}U$ ratios were measured in samples delivered to the University of Wyoming using a Thermo-Finnegan Neptune multi-collector, inductively coupled plasma, mass spectrometer (MC-ICP-MS) in the UW radiogenic isotope lab. Prior to mass spectrometer analysis, the samples required significant chemical preparation in a class 100 clean lab environment. A double U spike (IRMM 3636, a mix of ^{233}U-^{236}U) was added prior to evaporation, so that any induced isotopic fractionations could be tracked through all chemical processing, ion exchange purification and mass spectrometry. IRMM 3636 was prepared by the Joint Research Center of the European Commission. It has been carefully calibrated with a measured $^{233}U/^{236}U$ of 1.01906 (Richter *et al.*, 2008) and the abundances of ^{235}U and ^{238}U are low, although they were corrected for in the data reductions. Precise $^{238}U/^{235}U$ and $^{238}U/^{234}U$ measurements require accurate monitoring of analytical fractionation, especially during mass spectrometry. IRMM 3636 was prepared specifically for this use.

Appropriately sized aliquots of uranium samples were evaporated to yield 100 nanograms or more of uranium. These samples were then cleaned on ion exchange columns, using well-tested, published procedures (HCl-HNO_3-H_2O) and Eichrom anion resin. Total procedural blanks were less than 10 picograms uranium (sample to blank ratio of 10,000 or more), so no blank corrections were made to the results.

For the mass spectrometry measurements, an Airidus desolvating nebulizer was used to dry the plasma and increase signal strengths. MC-ICP-MS analyses were run in multi-collector, Faraday static mode with signal intensities of ≥11V ^{238}U (typically 20V) and at least 80 mV ^{235}U (typically 140 mv), sufficiently high to overcome signal to noise limitations for ^{235}U. ^{234}U signals were measured in a Faraday collector for the 7P-129 samples, with typical intensities of 2 mv. An ion counting multiplier was used for ^{234}U signals from the 7P-29 and 7P-30 samples with typical intensities of 30k to 60k counts per second. Uranium standards NIST 960, a solution with natural $^{238}U/^{235}U$, and NIST U010, a synthetic solution with $^{238}U/^{235}U$ of 98.6, were run to determine long-term reproducibility and stability of the mass spectrometer. Both standard bracketing and spiked-standard runs were performed to determine the effectiveness of fractionation measurements by each method. External reproducibilities based on these standard measurements averaged ±0.01% (2 sigma) for $^{238}U/^{235}U$, ±2% (2 sigma) for $^{238}U/^{234}U$. Samples were spiked with IRMM 3636 for a $^{238}U/^{236}U$ of approximately 12. Tail corrections were based on linear fits between measured 1/2 mass baselines. Corrections for ^{238}U, ^{235}U and ^{234}U contributed from the IRMM 3636 spike were made offline.

Field Test Results

Cross-Well Tracer Tests

The fluorinated benzoate tracer breakthrough curves in the two five-spot patterns are shown in Fig. 6. The tracer concentrations in Fig. 6 are normalized to the mass of tracer injected (units of concentration per kg injected), and they are shown as a function of volume produced at

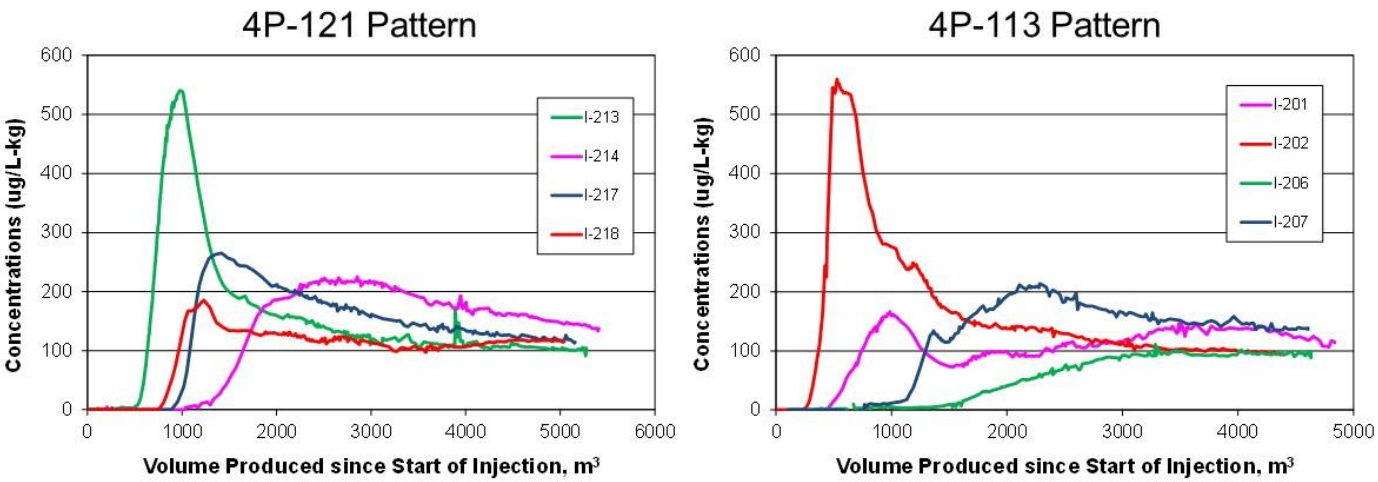

Figure 6. Normalized breakthrough curves of fluorinated benzoates in the two test patterns. All curves are shifted so that zero volume corresponds to when each tracer injection started.

the production wells *since the start of each respective tracer injection*. That is, the x-axes of the breakthrough curves are adjusted to reflect what would have been observed if all the tracer injections had started at the same time. Breakthrough curves were also obtained for the iodide that was injected into each of the corner wells in each pattern, and these normalized breakthrough curves are shown in Fig. 7 along with the *sum* of the fluorinated benzoate curves. In this case, the fluorinated benzoate curves are not adjusted to all start at the same time because the iodide was injected at different times and its response from any given injection well cannot be distinguished from the responses from the other injection wells, so there is no way to make a well-specific correction as for the benzoates.

It is apparent from Fig. 7 that the breakthroughs of the iodide correspond very well with the breakthroughs of the fluorinated benzoates during the early part of the tests in each pattern. This result is important because there was a concern that the fluorinated benzoates might have adsorbed weakly to organic material in the aquifer that is known to be present in the roll-front deposits at Smith Ranch-Highland. Such adsorption had previously been observed in laboratory column experiments conducted at Los Alamos using material from a corehole drilled into the 4P-121 pattern prior to the field tests (see Fig. 3 for location of this hole). However, the lab tests were thought to be potentially biased because organic-rich material from the corehole was over-represented in the columns to increase the chances of seeing interactions between the fluorinated benzoates and the aquifer material. Breakthrough curves from these experiments are shown in Fig. 8, and they indicate that the transport of the fluorinated benzoates through the column were retarded relative to iodide, which should not interact at all with organic material. The fluorinated benzoate retardation was reproducible, and the four benzoates showing the least amount of retardation relative to iodide were selected for field testing. The fact that the sum of the benzoate breakthrough curves is in good agreement with the early iodide breakthrough curve in each well pattern (Fig. 7) indicates that there was little or no apparent adsorption of the benzoates in the field tests, and thus no corrections to the benzoate breakthrough curves to account for adsorption were necessary. These results also suggest that the flow pathways that that tracers followed must have had very little organic material in them relative to the organic content of the laboratory column.

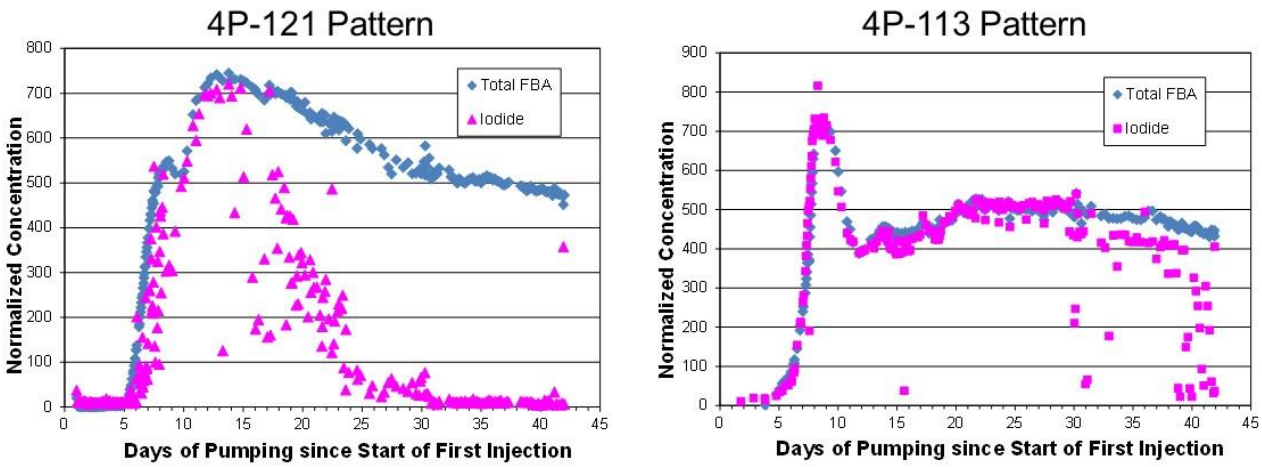

Figure 7. Normalized breakthrough curves of the *sum* of the fluorinated benzoates and iodide in the two test patterns. Note that x-axis is time and time zero corresponds to the start of the first tracer injection.

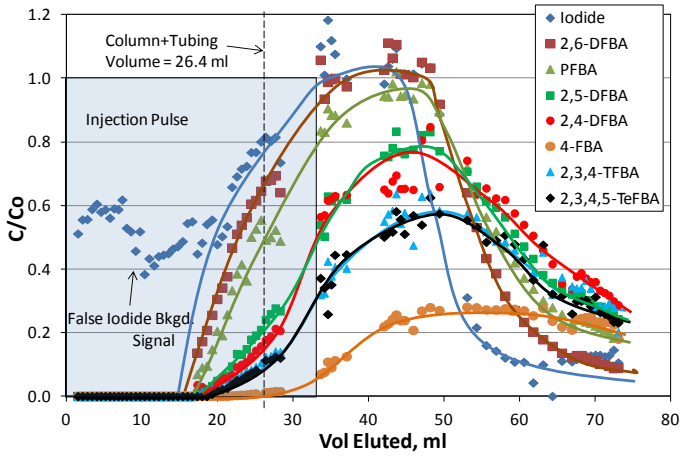

Figure 8. Normalized breakthrough curves of several fluorinated benzoates and iodide in a laboratory column experiment using organic-rich material from the corehole drilled into the 4P-121 pattern (see Fig. 3). The four FBAs showing the least amount of retardation relative to iodide were selected for the cross-well tracer tests.

A second key observation with the iodide breakthrough curves relative to the fluorinated benzoates in Fig. 7 is that the iodide tended to disappear from the patterns late in the tracer tests. This disappearance is consistent with the oxidation of iodide to iodine (or possibly even to an oxyanion of iodine, e.g., iodate), which is not surprising given that the tracer tests were conducted in ore zones that had been heavily oxidized by introduction of O_2 during previous mining operations. The introduction of O_2 would have oxidized many minerals present in the ore zone besides uranium-bearing minerals. Reduced iron phases known to exist in the ore zone (e.g., pyrite) would have been oxidized to ferric oxides or ferric oxyhydroxides, and these minerals could have accepted electrons from iodide, resulting in oxidation of the iodide. It appears that more phases capable of oxidizing iodide were present in the 7P-121 pattern than in the 7P-113 pattern. Although not an objective of this study, the results of Fig. 7 suggest that iodide might

serve as a useful probe of redox conditions in previously-mined ore zones, and perhaps could provide an indication of how reduced a previously-oxidized zone has become after some sort of remediation treatment.

Single-Well Push-Pull Tests

The 'return curves' of the tracers and uranium in the single-well push-pull tracer tests are shown in Figs. 9 through 11 for the tests in 7P-129, 7P-30, and 7P-29, respectively (note that the concentrations are normalized by dividing by the injection concentrations, and the uranium concentrations are background-subtracted). The calculated recoveries of the tracers and uranium are shown as a function of volume pumped in the right-hand plots of Figs. 9-11. A curve is included for chloride in each figure because the chloride concentrations in the MU-4A waters were much higher than the background concentrations in the MU-7 wells, so chloride (after background subtraction) effectively served as an additional nonreactive tracer. Chloride has very low background concentrations in Smith Ranch-Highland waters but because it is the anion that exchanges for uranium carbonate in the ion exchange resins used at the facility, it tends to build up significantly in mined ores zones.

Two curves are shown for uranium in each of Figs. 9 to 11; one for bulk uranium concentrations and one for uranium concentrations that are estimated to have been contributed from the MU-4A injection waters. The difference between the two curves is assumed to be uranium that was inadvertently mobilized from the MU-7 ore zone as a result of the push-pull tests. The contribution from mobilized uranium was deduced to be quite significant in all the tests and especially in the 7P-29 test, which had the low-uranium 4P-61 injection water. The differentiation between injected uranium and uranium derived from the ore zone was made using the $^{234}U/^{238}U$ activity ratios of the injection, chase and background waters, with the assumption that any uranium mobilized from the ore zone had the same isotopic ratio as the background water in any given well. The $^{234}U/^{238}U$ activity ratios in each of the well waters are listed in Table 5. The background ratios in the push-pull wells were taken to be the activity ratios measured in the last sample collected from each of the tests, after bulk uranium concentrations had effectively reached background levels. It is apparent from Table 5 that there is a striking difference between the activity ratios in the MU-4A injection waters and the MU-7 background waters in the targeted injection wells. It is also somewhat fortuitous that the ratio in the 7P-38 chase water was similar to that in the MU-4A waters, which allowed the uranium in the chase water to be lumped with the uranium in the MU-4A injection waters when doing the mixing calculations to estimate relative contributions from the injection waters and the ore zone.

Figs. 12 to 14 show the $^{234}U/^{238}U$ activity ratios in samples from the three push-pull tests as a function of volume pumped; note that many fewer samples were analyzed for activity ratios in each test than for elemental concentrations because of the much greater expense associated with the isotope ratio measurements. Also shown in Figs. 12 to 14 are the fractions of recovered uranium estimated to have come from the injection waters as a function of volume pumped in each test. These fractions were estimated as follows:

$$Fraction = \frac{(Activity\ ratio\ in\ sample - Background\ activity\ ratio\ in\ well)}{(Activity\ ratio\ in\ injection\ water - Background\ activity\ ratio\ in\ well)} \quad (1)$$

There are no available data to support the assumption that the activity ratio of uranium mobilized from the ore zone was the same as the ratio in the background water from each MU-7 well. However, if the activity ratio of mobilized uranium was lower than in the background waters (as

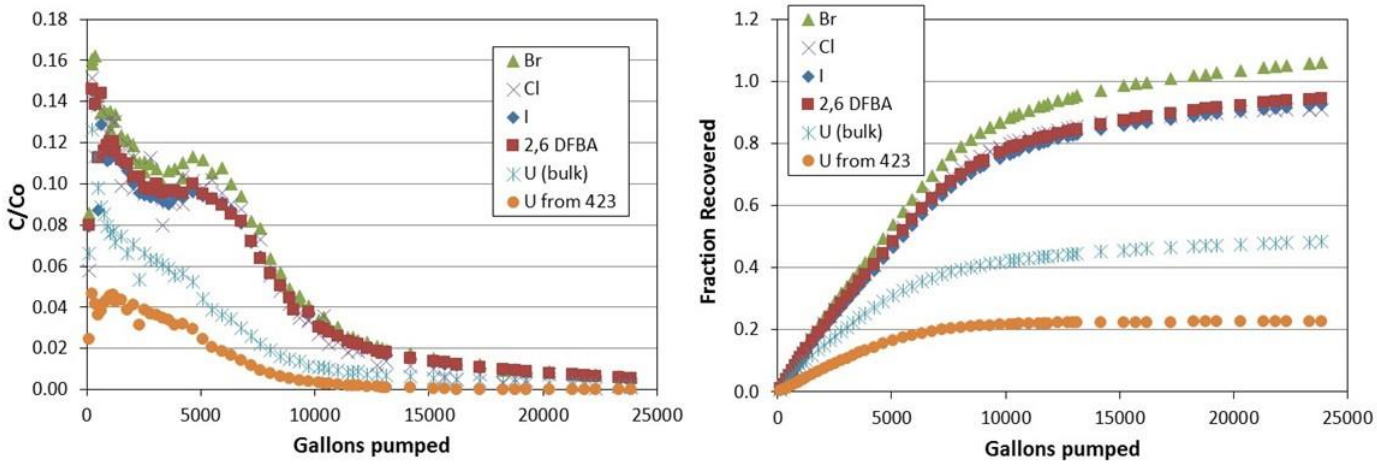

Figure 9. Normalized return curves and recoveries of nonreactive tracers and uranium in 7P-129 push-pull test. '423' refers to well MP-423.

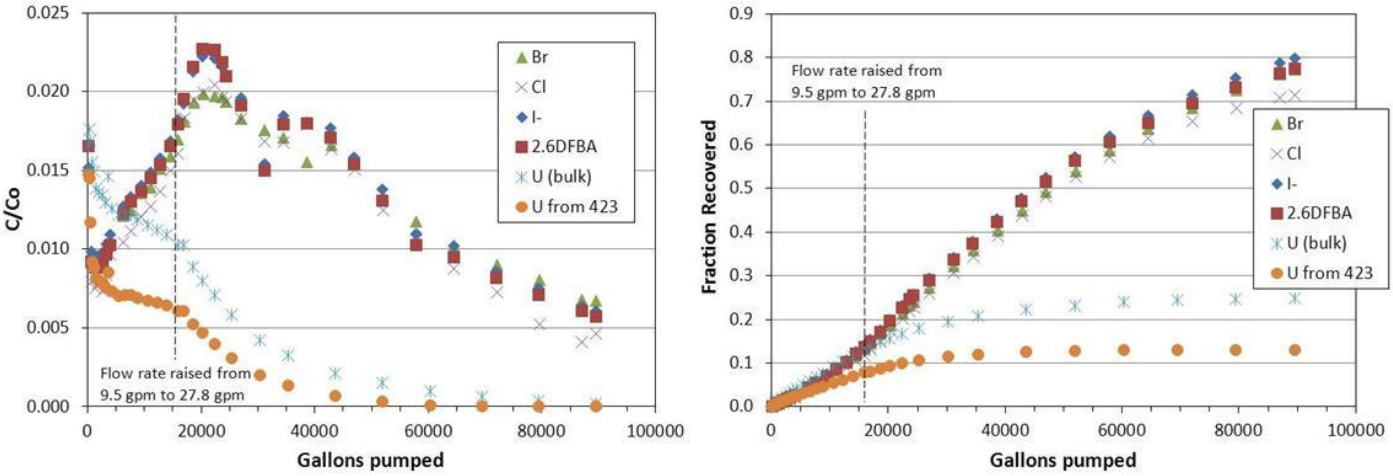

Figure 10. Normalized return curves and recoveries of nonreactive tracers and uranium in 7P-30 push-pull test. '423' refers to well MP-423.

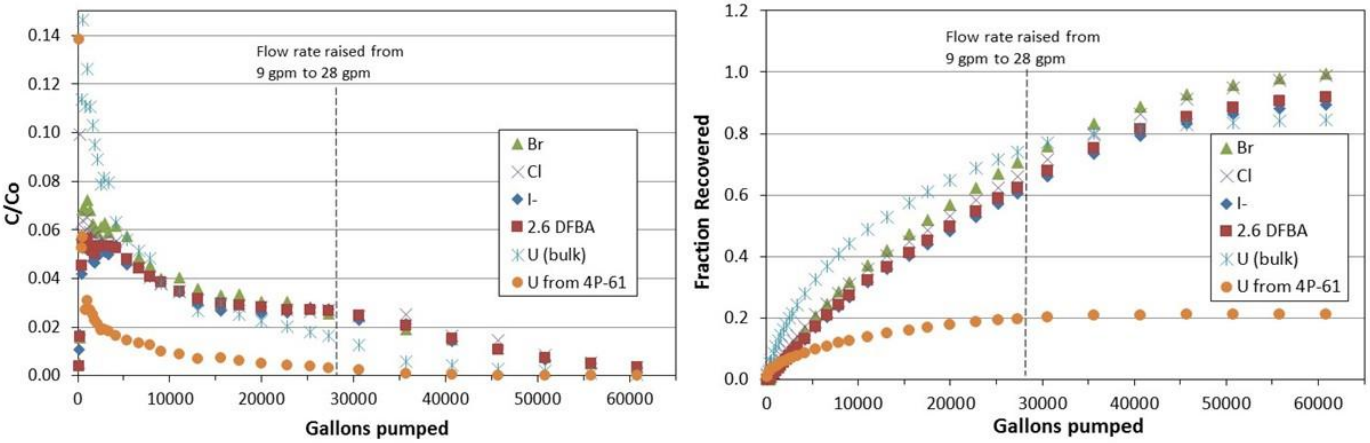

Figure 11. Normalized return curves and recoveries of nonreactive tracers and uranium in 7P-29 push-pull test.

Table 5. $^{234}U/^{238}U$ activity ratios in well waters used in the push-pull tests.

Well	$^{234}U/^{238}U$ activity ratio
MP-423 (Injected Water)	1.12
4P-61 (Injected Water)	1.085
7P-38 (Chase Water)	1.025
7P-129 (Push-Pull Well)	1.375
7P-30 (Push-Pull Well)	1.52
7P-29 (Push-Pull Well)	2.60

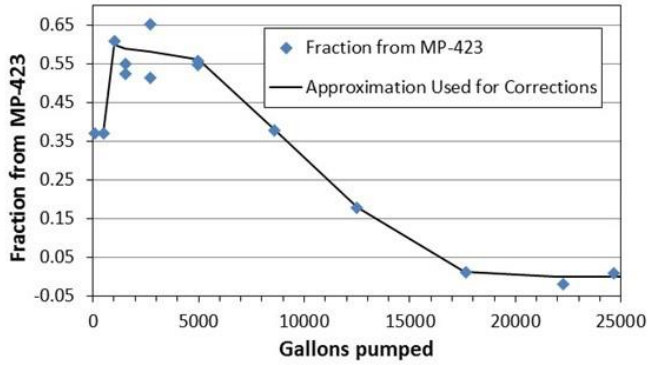

Figure 12. Fractions of recovered uranium attributable to MP-423 injection as a function of volume pumped in 7P-129 push-pull test based on $^{234}U/^{238}U$ activity ratio mixing calculations.

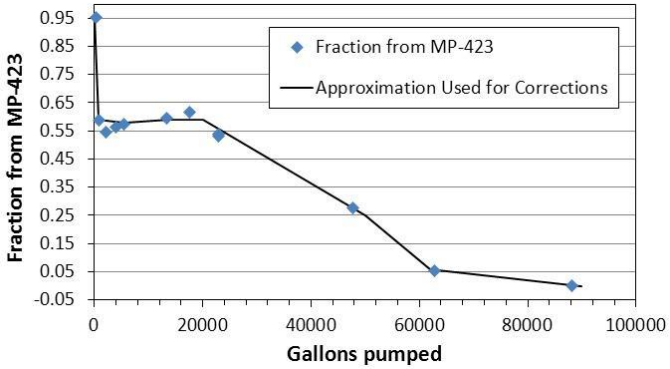

Figure 13. Fractions of recovered uranium attributable to MP-423 injection as a function of volume pumped in 7P-30 push-pull test based on $^{234}U/^{238}U$ activity ratio mixing calculations.

might be argued based on the low activity ratios in the post-mined waters from MU-4A), then the uranium contributed from the ore zone would constitute a *greater* fraction of the uranium recovered, and it follows that the contribution from the injected waters would be less than that indicated in Figs. 9-11. Thus, if the assumption that the mobilized uranium has the same activity ratio as in the background waters is incorrect, the injected uranium recovery would be overestimated and the attenuation of injected uranium would be underestimated. It is also implicitly assumed that there is insignificant fractionation of uranium isotopes in whatever process(es) are causing the attenuation of the injected uranium, which is a reasonable assumption if adsorption is the dominant process because adsorption is not believed to cause isotopic fractionation.

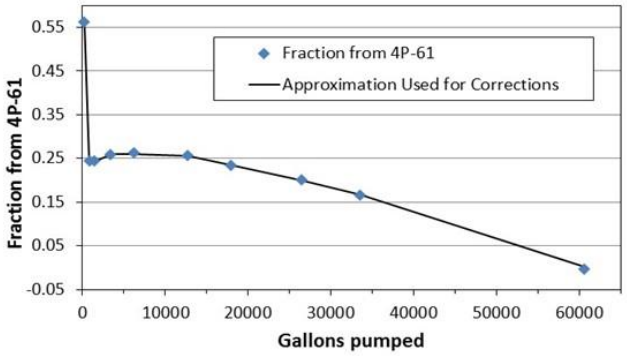

Figure 14. Fractions of recovered uranium attributable to 4P-61 injection as a function of volume pumped in 7P-29 push-pull test based on $^{234}U/^{238}U$ activity ratio mixing calculations.

Table 6 lists the nonreactive tracer and uranium recoveries (both total and fraction of injected uranium) in each of the push-pull tests. In addition to the recoveries at the end of pumping, the recoveries of the nonreactive tracers estimated from log-linear extrapolations of the tails of the breakthrough curves are provided. A log-linear extrapolation (a linear extrapolation of log concentrations vs. volume pumped) is a widely accepted method of extrapolating tracer breakthrough curves for the purposes of estimating moments of the curves or tracer recoveries that would have occurred if tests had been conducted longer. In all the tests, the extrapolated nonreactive tracer recoveries were estimated to be very close to 1.0, which is reassuring because this is the theoretical recovery in a well-behaved single-well push-pull test. The uranium recoveries on the other hand are significantly less than 1.0, and they do not increase much with extrapolation because the concentrations are already at or very close to background concentrations at the end of each test.

It is noteworthy that the highest uranium concentrations in each of the push-pull tests were observed immediately after pumping started, and even the nonreactive tracer concentrations were highest immediately after pumping started in 2 of the 3 tests. Only in the 7P-30 test did the nonreactive tracer concentrations start out lower and increase to a peak that occurred well after pumping started. This behavior, particularly for the nonreactive tracers, was unexpected considering that each of the tracer injections was followed with a significant amount of tracer-free chase water, and the ambient flow velocities in the ore zone were thought to be very low (7-10 feet per year). At a minimum, it was expected that tracer concentrations would not peak until at least half the chase volumes had been withdrawn from the wells.

Table 6. Calculated nonreactive tracer and uranium fractional recoveries in the push-pull tests.

	--------- At End of Pumping ----------			---------- Extrapolated ----------		
Constituent	**7P-129**	**7P-30**	**7P-29**	**7P-129**	**7P-30**	**7P-29**
2,6 DFBA	0.946	0.774	0.919	0.995	0.941	0.95
Iodide	0.925	0.797	0.895	0.974	0.99	0.927
Bromide	1.06	0.773	0.994	1.11	0.994	1.025
Chloride	0.92	0.715	0.988	-	-	-
Total Uranium	0.483	0.249	0.844	0.498	0.253	0.848
Injected Uranium	0.225	0.130	0.213	0.225	0.130	0.213

Note: Chloride extrapolation was not calculated because of significant background concentration.

The best explanation that can be offered for the earlier-than-expected tracer arrivals in the push-pull tests is that there was different spatial distribution of flow out of the wellscreens into the aquifer when the solutions were injected than when water was drawn out of the aquifer during pumping. This explanation may seem counterintuitive, but it is suggested by the difficulty encountered while injecting the MU-4A waters and 7P-38 chase water into the MU-7 wells. The injections and chase into both 7P-129 and 7P-30 had to be done in stages because the back pressure kept building to the maximum allowable wellhead pressure of 120 psig in both wells, and it took more than 3 days to finish the chase into 7P-129. Gas was bled off the 7P-129 wellhead several times during the injection/chase into this well, which suggested that either the injection solutions were degassing, or perhaps air was being entrained as the solutions were flowing into the well. The backpressure problems were not nearly as bad for the 7P-29 injection and chase, although there was still an early arrival of nonreactive tracers when this well was pumped back.

Fig. 15 provides a conceptual sketch that might explain the early tracer arrivals. During injection, 'gas lock' may have occurred in some sections of the wellscreen (most likely the upper portions) that would have otherwise accepted significant amounts of water if the gas had not been present. This 'locking' resulted in tracers and uranium penetrating only a short distance into the aquifer in these sections during the injection and chase. However, when the flow was reversed during pumping, the sections that were 'locked' during injection would have flowed freely and the tracers and uranium that had penetrated only a short distance into the aquifer would have returned very quickly. On the other hand, tracers that penetrated large distances into the aquifer during injection (in wellscreen sections that were not gas locked) would have returned much more slowly than expected because these sections would have contributed less flow during pumping than during injection. These slow returns are reflected in the estimated mean pumping volumes for the nonreactive tracer returns (the volumes associated with the 'center of mass' of the tracer

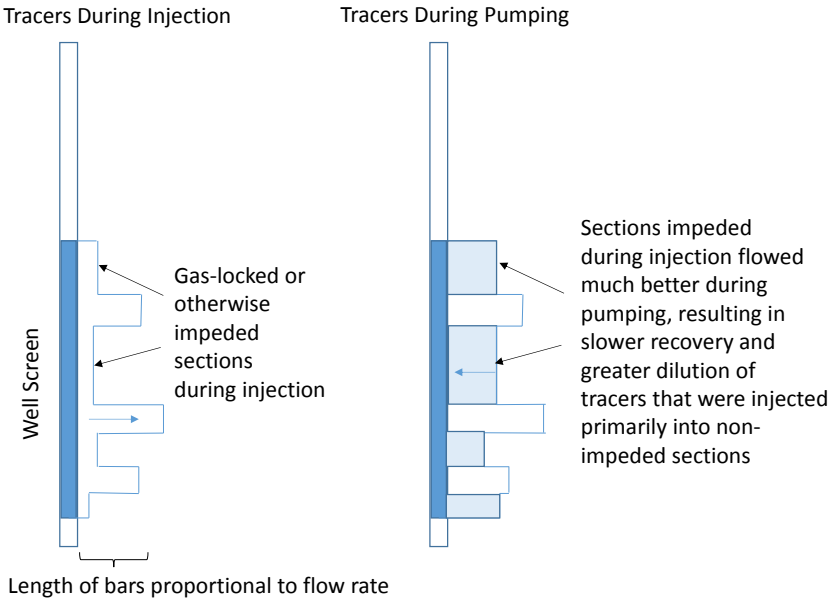

Figure 15. Conceptualization of flow differences during injection and pumping that may explain early nonreactive tracer arrivals.

returns, calculated using the extrapolated breakthrough curves), which are listed in Table 7 for each of tests, along with the theoretical mean volumes that are equal to the chase volumes plus half the injection volumes. The difference between the observed and theoretical mean pumping volumes can be used to estimate how far the tracers 'drifted' in the aquifer under the influence of natural gradient flow during the time when there was no injection or pumping. The details of how these estimates are calculated are not provided here, but they result in natural flow velocity estimates of 68 ft/yr, 30 ft/yr and 23 ft/yr for wells 7P-30, 7P-129, and 7P-29, respectively. All of these estimates are much higher than the ~10 ft/yr that the hydrology data from MU-7 suggest (Norwest Corp, 2013), which is consistent the hypothesis that some of the tracer mass returned much more slowly than expected because of the explanation provided above. We have no way of verifying this hypothesis, and it is possible that the higher estimated flow rates reflect the influence of ISR mining activities that were occurring in nearby areas, but the tracer data and injection difficulties suggest that the above explanation is quite plausible.

The remaining data from each of the three push-pull tests are plotted in Appendix C. These data, which are not discussed further in any detail in this report, include:

- The YSI-meter-recorded values of specific conductance, pH and ORP (mV vs. Ag/AgCl electrode) during pumping.
- The major cation data from ICP-OES during pumping.
- The minor/trace element data from ICP-MS during pumping
- The major anion data from ion chromatography during pumping
- Charge balance data during pumping based on the major cation and anion data; the positive charge excess can be used to estimate the HCO_3^- concentrations and alkalinity.
- HCO_3^- concentrations and alkalinity during pumping, with field alkalinity measurements also plotted for comparison.
- $^{238}U/^{235}U$ ratios during pumping, which did not show evidence of biotic uranium reduction processes occurring during the tests. We note that the lack of a significant shift in $^{238}U/^{235}U$ ratios during the tests does not rule out the possibility of abiotic reduction processes, as recent studies have suggested that variations in $^{238}U/^{235}U$ in low temperature environments arise primarily due to direct enzymatic uranium reduction by microbes and that $^{238}U/^{235}U$ is not significantly fractionated by inorganic reduction (Stirling et al., 2015; Stylo et al., 2015).

It is noteworthy that he pH in two of the wells (7P-129 and 7P-30) was initially high but dropped rapidly, which probably reflects some grout in these well completions that caused local increases in pH while the wells sat idle. These high pHs may have also affected the initial uranium concentrations in the wells, as uranium is much more resistant to adsorption at high pH than at lower pH if the alkalinity is the same (higher pH results in increased complexation of uranium to carbonate). The specific conductance in the tests generally follows the trends of the nonreactive tracers. The ORP in all tests rapidly decreased to very low levels, although the levels were notably lower in the 7P-129 test than in the other two tests.

Table 7. Observed and theoretical mean pumping volumes in each of the push-pull tests.

Push-Pull Well	Observed	Theoretical
7P-129	7500	5230
7P-30	58,000	5830
7P-29	22,000	6680

Perhaps the constituent concentration data of greatest interest from the three push-pull tests, other than uranium and the tracers, is that for the elements Se, As, and V. Se and As are both potential problem constituents that are mobilized during ISR mining, and V has geochemical behavior similar to that of uranium and can thus serve as a reasonable proxy for ore zone uranium. Figs. 16 to 18 show the concentrations of these elements as a function of volume pumped during each of the respective tests.

Although it was initially hoped that the push-pull tests might provide useful information on the downgradient attenuation of Se and As, it is quite evident that considerable amounts of both elements were liberated from the MU-7 ore zone during the tests. The concentrations of these elements reached levels that exceeded the concentrations in both the injection waters and in the chase water, at least during the early part of each test. One must conclude that the ore zone was contributing the majority of these elements in the pumped waters, and thus it is not possible to evaluate their attenuation from these data. Vanadium was also apparently liberated early in the tests, which is consistent with the liberation of uranium from the ore zone that was deduced from the $^{234}U/^{238}U$ activity ratios. The V data qualitatively support the activity ratio corrections that were made to distinguish between injected and ore zone uranium.

The results of Figs. 16 to 18, in conjunction with the uranium data, suggest that it is very difficult to avoid some inadvertent oxidation of the ore zone when waters are injected into it, even when an attempt is made to avoid introducing O_2. However, the ore zone oxidation appears to be limited to quite near the injection well because the elevated levels of constituents like Se and V, which are only mobile when oxidized, do not persist for long. Thus, O_2 or other oxidants in the injected waters must be rapidly consumed as the oxygenated water flows into the aquifer. Unlike Se, V and uranium, As is generally more mobile in groundwater when it is in a reduced state than in an oxidized state. Thus, it is difficult to attribute the apparent mobilization of As to oxidation of the ore zone, but rather it must have been caused by some other process, perhaps interactions with reductants present in the injected waters. If attenuation data for Se or As are desired in push-pull tests, it would seem necessary to spike the injected waters with these elements to ensure that their return concentrations greatly exceed the concentrations that are liberated from the ore zone. With uranium, the activity ratios appear to be a promising tool for distinguishing between injected uranium and mobilized uranium, provided a sufficient contrast exists between the two sources of uranium. Stable isotopes of Se and As might also be considered for spiking injection solutions if they are available at reasonable cost and analytical costs are not high.

Because of the inability to estimate attenuation parameters for Se and As in the push-pull tests, only the downgradient attenuation of uranium was ultimately predicted from the information generated in this study.

Field Test Interpretations

Cross-Well Tracer Tests

The first step in the interpretation of the cross-well tracer tests was to deconvolute the effects of recirculation on the tracer breakthrough curves. The fully-recirculating configuration of the tests meant that tracers arriving at the production well were immediately reinjected into all four corners of the pattern and began to move through the pattern again, and this process was repeated until the end of the test. To obtain unbiased estimates of swept volumes and sweep efficiencies in the patterns, and to estimate tracer dispersion due to flow heterogeneity in the aquifer, it is necessary to first mathematically remove the effects of recirculation from the

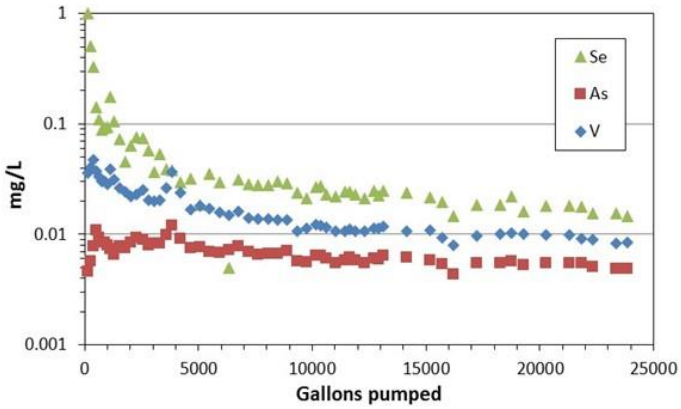

Figure 16. Concentrations of Se, As, and V during pumping in the 7P-129 push-pull test. Injection concentrations were: Se = 0.051, As = 0.002, and V = 0.012 (mg/L). Chase water concentrations were: Se = 0.1, As = <0.002, and V = 0.014 (mg/L).

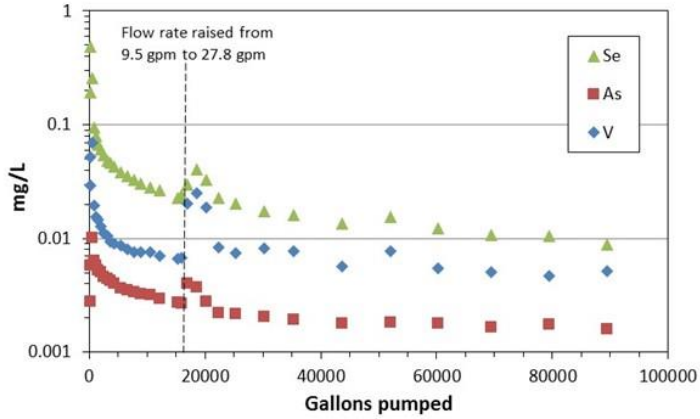

Figure 17. Concentrations of Se, As, and V during pumping in the 7P-30 push-pull test. Injection concentrations were: Se = 0.051, As = 0.002, and V = 0.011 (mg/L). Chase water concentrations were: Se = 0.1, As = <0.002, and V = 0.014 (mg/L).

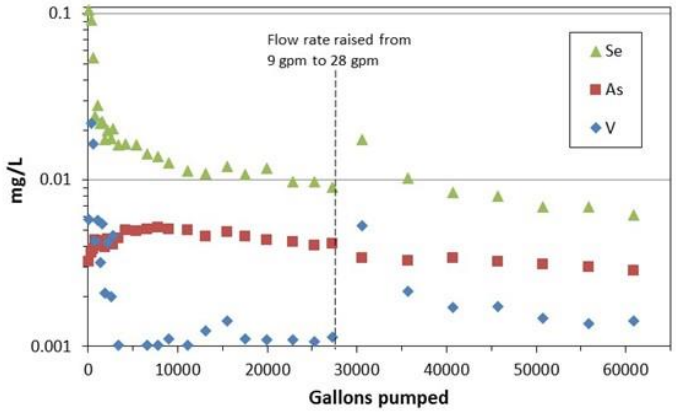

Figure 18. Concentrations of Se, As, and V during pumping in the 7P-29 push-pull test. Injection concentrations were: Se = 0.066, As = 0.015, and V = 0.005 (mg/L). Chase water concentrations were: Se = 0.1, As = <0.002, and V = 0.014 (mg/L).

breakthrough curves and, in effect, determine what the breakthrough curves would have looked like if the tracers had been magically removed from the produced water before the water was recirculated. Such hypothetical breakthrough curves are referred to here as 'once-through' breakthrough curves.

The once-through breakthrough curves were obtained using a method that, to our knowledge, has not been previously reported or implemented. The method involves the use of Laplace transforms and Laplace transform inversions and is loosely based on the concepts of the RELAP model developed for tracer test interpretations and described in Appendix A of Reimus et al. (2003). For convenience in using the Laplace transform method, each of the observed breakthrough curves was discretized into 101 equally-spaced volume increments. In the Laplace domain, this is represented as

$$f_{BT}(s) = \sum_{i=1}^{101} C(i)\Delta t\, e^{-t_i s} \qquad (2)$$

where, $f_{BT}(s)$ = Laplace transform function for observed normalized tracer breakthrough curve,
$C(i)$ = tracer concentration at *i*th time increment, μg/L-kg injected
Δt = time increment used for discretization,
t_i = time associated with *i*th time increment, hrs
s = Laplace variable (replacing time as independent variable).

For a recirculating system with four injection wells and one production well, it can be shown that the composite (i.e., observed) Laplace-domain breakthrough function for a tracer injected into a given injection well *i* is given by:

$$f_{BT_i}(s) = \frac{f_{BT_{i,1}}(s)}{1-\sum_{j=1}^{4} \varepsilon_j\, f_{BT_{j,1}}(s)} \qquad (3)$$

where, $f_{BT_i}(s)$ = Laplace-domain composite breakthrough curve function for *i*th tracer or injection well,
$f_{BT_{i,1}}(s)$ = *Once-through* Laplace-domain breakthrough curve function for *i*th tracer or injection well
ε_j = recirculation ratio for *j*th injection well (i.e., fraction of production flow injected into jth injection well).

The Laplace-domain breakthrough functions (3) for each tracer (or injection well) can be inverted to the time domain using the numerical method given in Appendix A of Reimus et al. (2003), and the result will be a predicted tracer concentration at each of the 101 discretized time points of the original time discretization.

If the discretized *observed* breakthrough functions (2) for each tracer introduced into each injection well are inserted into equation (3) as once-through breakthrough functions, then the resulting inverted composite breakthrough curve for each tracer will overestimate the effects of recirculation by a significant amount because the effects of recirculation are already included in the observed breakthrough functions. However, if the observed concentrations are divided by the overpredicted concentrations at each discretized time point, and the resulting fraction is multiplied by the observed concentration, the result will be a *revised* (decreased) estimate of the once-

through concentrations that can be used in another iteration of the equation (3) inversion. For each successive iteration, the revisions to the once-through concentrations become smaller and each inversion of equation (3) results in a less overpredicted set of composite breakthrough curves. Eventually the revisions approach zero and the successive composite breakthrough curves converge to the observed breakthrough curves. The final revised once-through concentrations can then be taken as the best estimates of the actual once-through breakthrough concentrations. The Laplace domain inversions are very rapid because a highly optimized Fourier transform algorithm is used, as described in Reimus et al. (2003).

There are two key restrictions to the approach described above: (1) the flows must be relatively steady, with no change in the recirculation ratios, ε_j, during the test, and (2) the duration of the tracer injections must be relatively small compared to the first arrival times of the tracers. The steady flow restriction was circumvented by using the production volume as the independent variable instead of time (thus avoiding the complication of the flow interruptions due to power outages), and the recirculation ratios were considered steady enough to be assumed constant throughout the tests. The injection durations were never more than a factor of 2.4 less than the first arrival times of tracers, which was considered short enough to satisfy the injection duration restriction. With some effort, the method could be modified to relax the latter restriction. The resulting once-through breakthrough curves in the two well patterns are shown along with the observed breakthrough curves in Fig. 19.

After obtaining the once-through breakthrough curves, a log-linear extrapolation (linear extrapolation of log concentrations vs. volume) was applied to the curves to allow swept volumes and sweep efficiencies to be estimated for each pattern. The extrapolations are carried out until the area under the extrapolated curves no longer changes significantly with additional extrapolation. The swept volume is then calculated as follows:

$$V_{swept} = R\mu_{vol} \tag{4}$$

where, V_{swept} = swept volume, m^3,

R = extrapolated tracer recovery

$\mu_{vol} = \frac{\int_0^\infty C(V)VdV}{\int_0^\infty C(V)dV} - \frac{V_{pulse}}{2}$ (i.e., first moment of extrapolated breakthrough curve), m^3

$C(V)$ = normalized tracer concentration as a function of volume *injected* into injection well

V_{pulse} = volume of injection pulse, m^3.

Table 8 lists the once-through tracer recoveries and swept volumes associated with each injector-producer well pair, and it also lists the 'ideal' recoveries and swept volumes for each well pair that were calculated assuming that the aquifers in the patterns were perfectly homogeneous and isotropic. These calculations were done using a 2D numerical model; Fig. 20 shows an example of the area predicted to be 'swept' by tracers for the 4P-121 pattern using the homogeneous isotropic numerical model. The 'ideal' swept volumes and recoveries are not the same for each injector-producer well pair because the well patterns are not perfectly symmetrical, and the wellscreens are not same length in each well. The swept volumes and estimated tracer recoveries can be used to provide various measures of flow heterogeneity within the patterns, but instead of using these approaches, we used the concept of sweep efficiency to provide a measure of flow heterogeneity for use in predictions of downgradient transport of uranium. Sweep efficiency curves, or F-Φ curves as they are often called, were originally developed by the oil and

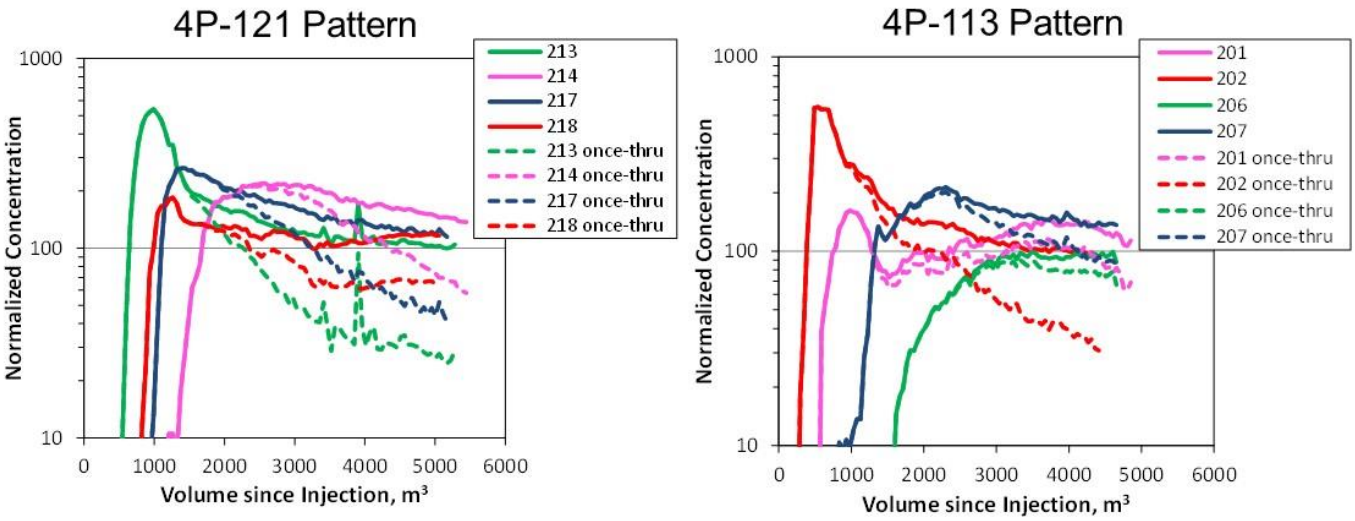

Figure 19. Observed and calculated once-through tracer breakthrough curves in the two cross-well test patterns. Note the log normalized concentration scales.

Table 8. Observed and ideal tracer recoveries and swept volumes in the two cross-well test patterns. Recoveries and swept volumes were estimated using log-linear extrapolations of once-through breakthrough curves.

Well-Pair	Obs. Recovery	Ideal Recovery	Obs. V_{swept}, m³	Ideal V_{swept}, m³
4I-213 / 4P-121	0.61	0.83	333	555
4I-214 / 4P-121	0.68	0.74	659	614
4I-217 / 4P-121	0.60	0.80	452	552
4I-218 / 4P-121	0.68	0.83	976	610
4I-201 / 4P-113	0.51	0.70	433	554
4I-202 / 4P-113	0.62	0.80	313	500
4I-206 / 4P-113	0.64	0.64	1282	576
4I-207 / 4P-113	0.73	0.79	841	510

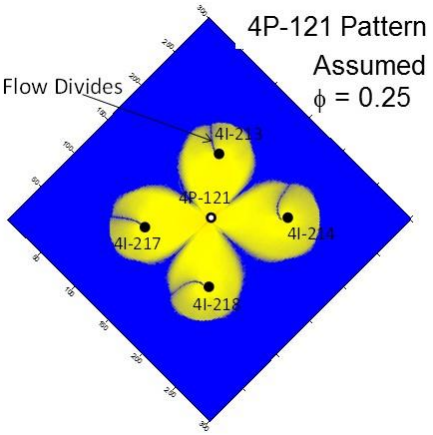

Figure 20. Plan view of 4P-121 pattern showing area swept by tracers in a 2-D simulation assuming homogeneous, isotropic and perfectly-confined flow.

gas industry for reservoir engineering (Lake, 1989). The flow capacity F and storage capacity Φ functions are calculated from once-through breakthrough curves, and they are defined as follows:

$$\text{Flow Capacity: } F(V) = \frac{\int_0^V C(V)dV}{\int_0^\infty C(V)dV} \quad (5)$$

$$\text{Storage Capacity: } \Phi(V) = \frac{\int_0^V C(V)VdV}{\int_0^\infty C(V)VdV} \quad (6)$$

where in this case *V* is the volume *produced* from the production well. When F is plotted against Φ (each F-Φ pair determined at a common volume, *V*), a curve such as that shown in Fig. 21 is obtained. The points on the curve increase in *V* from lower left to upper right. F is always greater than or equal to the corresponding value of Φ, and F can be interpreted as the fraction of volumetric flow that is occurring within a given fraction of flowing pore volume Φ (Fig. 21). For perfect piston-flow displacement (i.e., all pore volume transmits the same amount of flow), the values of F and Φ will always be the same and the F-Φ curve will be a diagonal line from (0,0) to (1,1) on the plot. The calculated F-Φ curves for the two cross-well test patterns are shown in Fig. 22. The curves of Fig. 22 were generated by inserting the *sum* of the once-through breakthrough curve data for each of the four injection wells into equations (x) and (y) so that a measure of sweep efficiency for the entire pattern would be obtained. Also shown in these figures are the F-Φ curves that would be obtained for the patterns if the aquifer was homogeneous and isotropic (calculated using the breakthrough curves predicted from the 2-D numerical model simulations). Note that these curves are not perfect diagonals because even in a homogeneous, isotropic system, the patterns have flow streamlines of varying lengths and some areas that see more flow than others, including stagnation points.

To obtain a measure of flow heterogeneity for use in downgradient transport calculations, it was considered necessary to subtract the F-Φ curves for the homogeneous, isotropic case for each pattern from the F-Φ curves that were obtained for each pattern using the observed breakthrough curve data. This process, in effect, subtracts out the apparent flow heterogeneity that is caused by the recirculating flows through the patterns. The resulting 'difference' F-Φ curves are shown in Fig. 23. These curves are probably skewed low at the upper right because the upper-right portion of the curves are based on volumes near the end of each test, where there is greater uncertainty in the deconvolution of the observed breakthrough curves to obtain the once-through breakthrough curves. Also, the once-through tracer recoveries for the observed and ideal cases diverge at late times/volumes, with the ideal recoveries being greater than the observed recoveries, which should increase the difference in the actual F-Φ curves relative to the apparent F-Φ curves (by using only the *recovered* tracer data in equations (x) and (y), the F-Φ curve for lower recovery cases will always be underestimated relative to higher recovery cases, particularly at the upper-right of the F-Φ curves).

The final step in the process was to use a simple 1-D advection-dispersion model (in this case, the RELAP code of Reimus et al., 2003) to generate hypothetical tracer breakthrough curves from which F-Φ curves could be calculated and compared to the difference curves of Fig. 23. The Peclet number, a dimensionless quantity equal to the length scale divided by the longitudinal dispersivity, was used as an adjustable parameter to obtain F-Φ curves that approximately

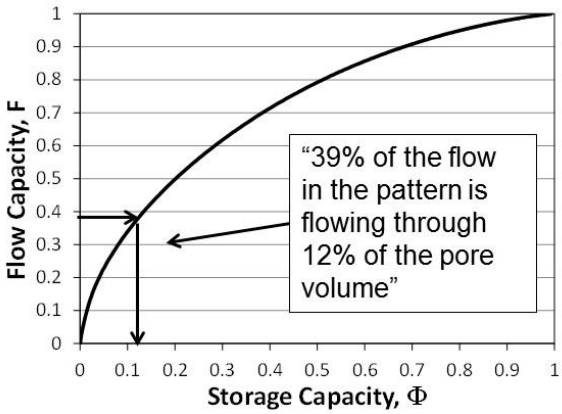

Figure 21. Example of F-Φ curve, illustrating how the curve is interpreted.

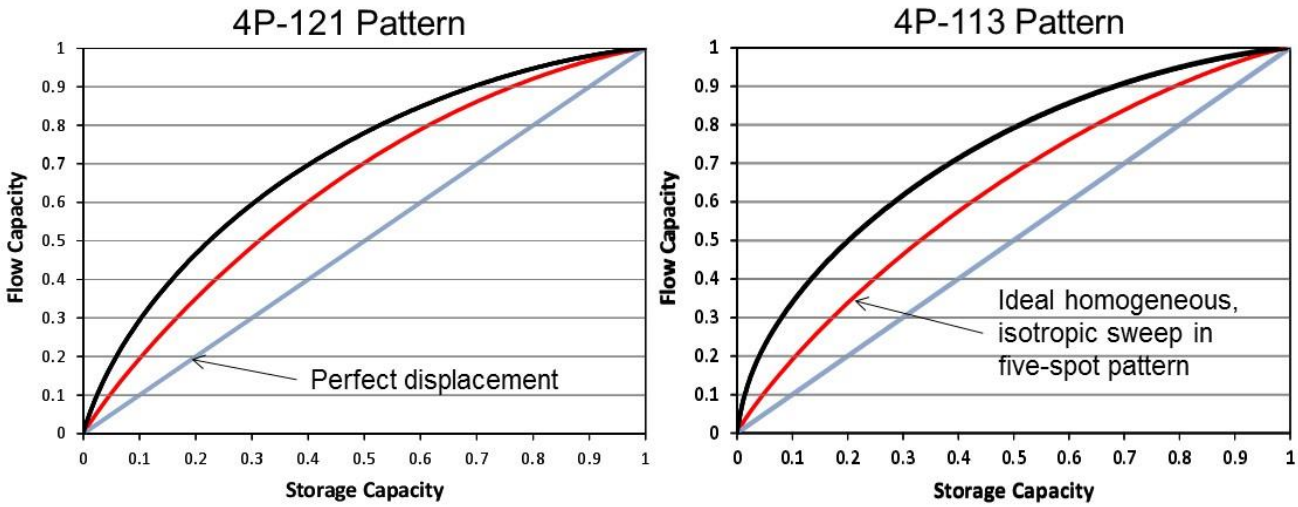

Figure 22. F-Φ curves for the two cross-well test patterns. Black is observed curves, red is ideal curve for a homogeneous, isotropic medium, and blue is perfect piston-flow displacement.

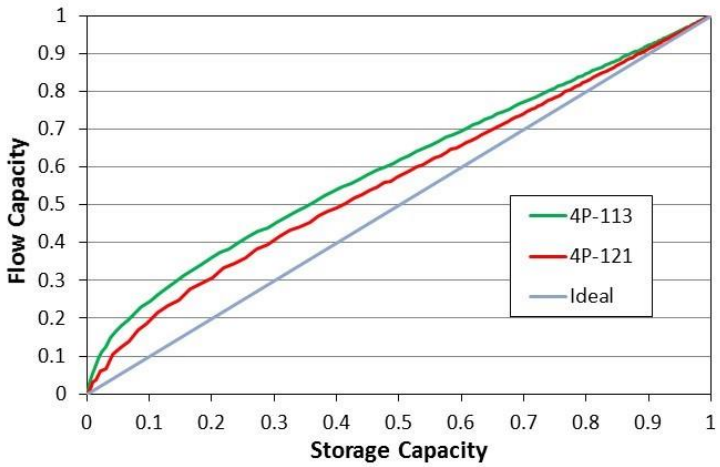

Figure 23. F-Φ curves for the two cross-well test patterns obtained after subtracting the observed curves from the ideal curves in Fig. 22.

matched the the lower-left portions of the difference curves. A F-Φ curve corresponding to a Peclet number of 8 was found to provide a reasonable match to the observed F-Φ difference curves, as shown in Fig. 24. Thus a Peclet number of 8, which corresponds to a moderate but not extreme amount of dispersion, was taken to be an appropriate Peclet number to use in subsequent downgradient transport predictions.

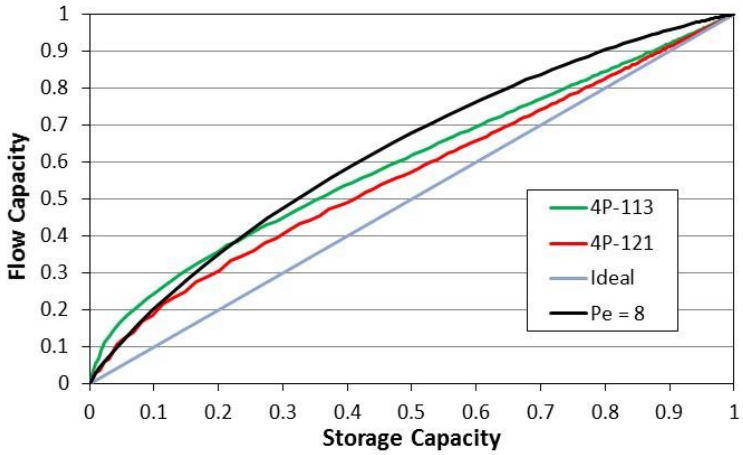

Figure 24. F-Φ curve for a Peclet number of 8 superimposed on the curves of Fig. 23.

Single-Well Push-Pull Tracer Tests

The push-pull tests were interpreted using a 1-D numerical model that simulates radial flow to and from a borehole with first-order reversible kinetic reactions to account for the reactive transport of uranium. The simulated reactions are generic, not mechanistic-based, and there are no accompanying geochemical calculations to account for interactions with specific mineral phases in the system or to simulate the space-time evolution of pH, alkalinity or other parameters that might affect uranium reactions. Irreversible attenuation processes such as reduction of U(VI) to U(IV) were not accounted for in the model, in part because there was no evidence of reduction during the push-pull tests based on the lack of a shift in $^{238}U/^{235}U$ ratios in the pumped waters (see Appendix C). However, by not allowing irreversible processes, the use of the deduced best-fitting model parameters to predict downgradient uranium transport made the predictions as pessimistic as possible (an irreversible process could only increase the predicted attenuation of uranium relative to a reversible process). The model also did not account for ambient flow in the aquifer during the idle period (when there is no injection or pumping).

Because of the unexpected early arrivals of the nonreactive tracers when the wells were pumped, it was not possible to reproduce the tracer breakthrough curves with the model using the actual injection and chase volumes/durations as model inputs. The model always predicted an initial increase in tracer concentrations until a peak was reached, which was when the volume produced approximately equaled the chase water volume plus half the injection volume. This inability to match the observed tracer breakthrough curves lends further support to the hypothesis that there were different flow conditions during injection and pumping, possibly due to 'gas locking' during injection.

Because the interpretations of uranium transport were highly dependent on comparisons of the uranium breakthrough curves to the nonreactive tracer breakthrough curves, it was considered necessary to force the model to match the observed nonreactive tracer breakthrough curves in

each test. This was accomplished by constructing artificial injection functions of varying concentration that effectively mimicked the observed breakthrough curves in reverse. That is, the first concentrations injected were the last concentrations to be observed during pumping and the last concentrations injected were the first concentrations to be observed during pumping. This approach required an injection/chase volume that equaled the volume pumped in each test, although the injections were still simulated as occurring over the actual injection times so that the simulated uranium reaction kinetics would occur over relevant time scales. To preserve the shapes of the tracer breakthrough curves, very small amounts of longitudinal dispersion were specified in the simulations.

A multi-site, multi-rate reaction model was used to simulate the reactive transport of uranium (Dittrich and Reimus, 2015). The applicable equations are:

$$\frac{\partial c}{\partial t} - v\frac{\partial c}{\partial r} + D\left(\frac{1}{r}\frac{\partial}{\partial r}\left(r\frac{\partial c}{\partial r}\right)\right) + \frac{\rho_B}{\emptyset}\left[-\sum_i k_{fi} c\left(1 - \frac{s_i}{s_{mi}}\right) + \sum_i k_{ri} s_i\right] \quad (7)$$

$$\frac{\partial s_i}{\partial t} = k_{fi} c\left(1 - \frac{s_i}{s_{mi}}\right) - k_{ri} s_i \quad (8)$$

where, c = uranium concentration in mobile aqueous phase, mol/ml
s_i = uranium surface concentration on adsorption site i, mol/g
t = time, hr
r = radial distance, cm
k_{fi} = adsorption rate constant for adsorption site i, ml/g-hr
k_{ri} = desorption rate constant for adsorption site i, hr^{-1}
s_{mi} = surface site abundance (maximum adsorption capacity) for adsorption site i, mol/g
v = flow velocity, cm/hr
D = dispersion coefficient, cm^2/hr
ρ_B = bulk density of aquifer, g/cm^3 (taken to be 2.65(1-0.25) = 1.99 g/cm^3 at Smith Ranch-Highland),
$\emptyset$ = porosity (taken to be 0.25 at Smith Ranch-Highland).

As the model interpretations were conducted, it was found that a minimum of three reactions were necessary to obtain reasonable matches to the recovery/breakthrough curves of uranium in each push-pull test. It was also found to be necessary to assume different reaction rates when the uranium was injected into the aquifer than when it was withdrawn. The latter was necessary because if the same rates were used during injection and recovery, the early recoveries of uranium were always significantly underestimated. In effect, the uranium was simulated as being more attenuated during the push into the aquifer than during the pull back out because this forced more uranium to remain near the well so that it could be recovered more quickly (as observed) during pumping of the well. The differences in kinetics during injection and withdrawal are not unreasonable, as the injection solutions had significantly different pH and alkalinity than the chase and background waters in the wells.

The model matches to the nonreactive tracer and uranium breakthrough curves in each of the push-pull tests are shown in Figs. 25 to 27. In all cases the model was matched to the activity-ratio-corrected uranium recovery curves that were believed to represent the return of *injected* uranium, with contributions from mobilized ore zone uranium removed. The reaction model parameters that produced the matches to the uranium curves of Figs. 25 to 27 are listed in Table 9.

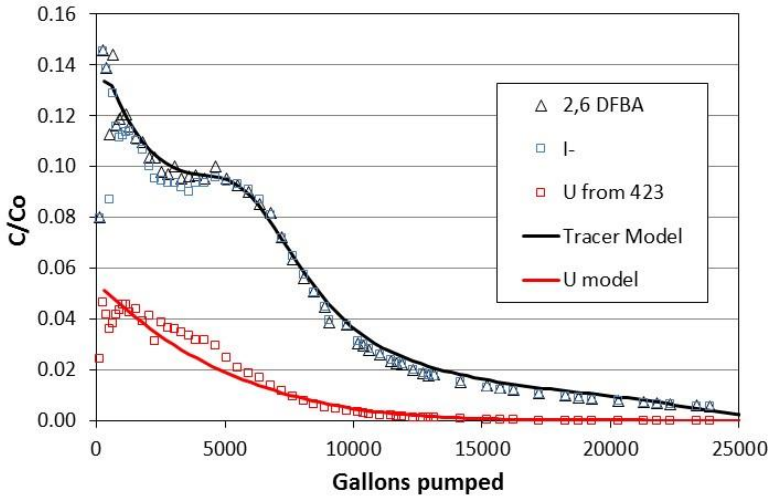

Figure 25. Model matches to 7P-129 push-pull test tracer and injected uranium recovery curves.

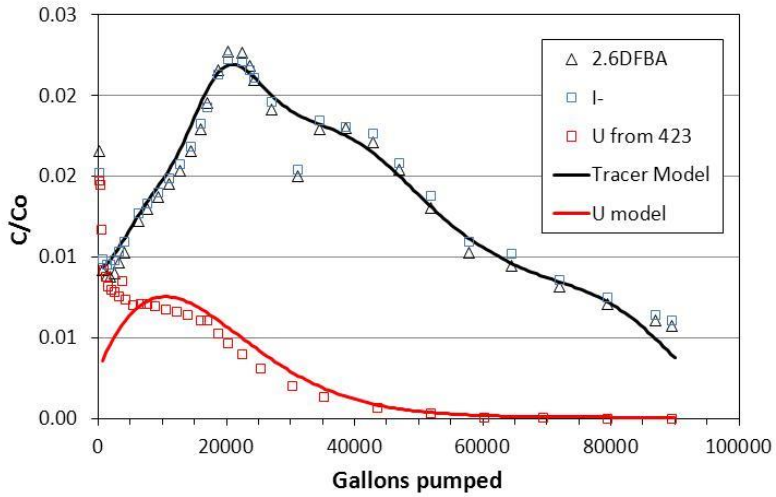

Figure 26. Model matches to 7P-30 push-pull test tracer and injected uranium recovery curves.

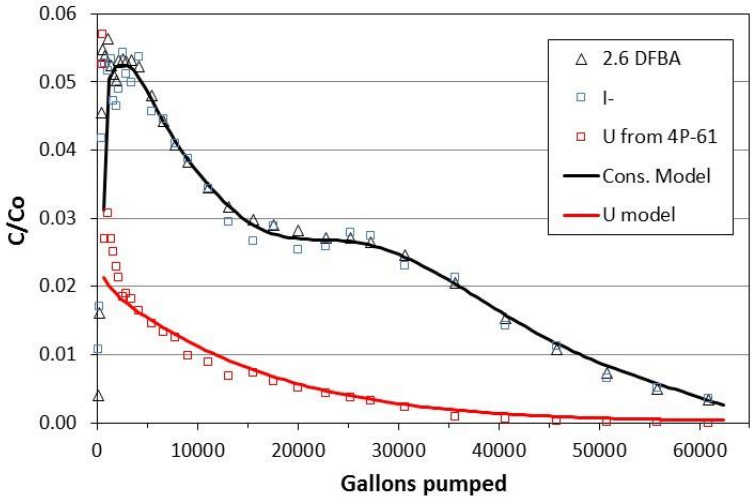

Figure 27. Model matches to 7P-29 push-pull test tracer and injected uranium recovery curves.

Table 9. Uranium reaction model parameters yielding the model curves of Figs. 25-27.

Parameter	7P-129 push	7P-129 pull	7P-30 push	7P-30 pull	7P-29 push	7P-29 pull
k_{f1}, ml/g-hr	5	5	5	5	8	8
k_{r1}, hr^{-1}	7	20	2.0	20	6.4	6.4
S_{m1}, µmol/g*	1.3	1.3	1.3	1.3	1.3	1.3
k_{f2}, ml/g-hr	2.5	2.5	2.5	2.5	4	4
k_{r2}, hr^{-1}	3.5	1.3	1.0	0.8	3.2	1.08
S_{m2}, µmol/g	0.067	0.067	0.067	0.067	0.008	0.008
k_{f3}, ml/g-hr	0.1	0.1	0.1	0.1	0.1	0.1
k_{r3}, hr^{-1}	0.05	0.0001	0.05	0.0001	0.0075	0.0001
S_{m3}, µmol/g	0.020	0.020	0.0111	0.0111	0.0011	0.0011

*This value was adjusted to be equal to the value suggested by Davis and Curtis (2003).

Note: Equivalent partition coefficients, or Kd values (ml/g), for *i*th adsorption site is equal to k_{fi}/ k_{fi}.

These parameters and the model interpretations are not claimed to be unique; in fact they are not unique. However, three reactions were definitely necessary to match the general characteristics of all the uranium breakthrough curves. The fastest reaction with the greatest abundance of adsorption sites accounted for the early arrivals of uranium, the second reaction with the intermediate reaction rates and intermediate abundance of adsorption sites accounted for the middle portion of the recovery curves, and the slowest reaction with the least number of sites effectively controlled the overall recovery of uranium and the late tailing behavior. The use of three reactions is consistent with the generalized composite surface complexation modeling approach taken by Davis and Curtis (2003) to describe uranium transport in shallow sediments at the Naturita, CO uranium mill tailings site. They used a three-site equilibrium model (no kinetics) with 'weak', 'strong', and 'very strong' sites that had successively lower abundances to describe uranium interactions with sediments in the Naturita system, although their approach incorporated more mechanistic geochemical dependencies than the simple approach taken here.

In the approach of this study, the model parameters that are the best constrained and ultimately have the greatest influence on uranium recoveries are the site abundance and the desorption rate constant of the *slowest* adsorption site. However, these two parameters were found to be negatively correlated in that the site abundance could be increased and the desorption rate constant decreased (and vice-versa) to yield approximately the same predicted late-time uranium breakthrough behavior. The approach taken here was to decrease the site abundance and increase the desorption rate constant as much as possible and still achieve a good match to the late-time data because this is the most conservative combination of parameter values from the standpoint of predicting the *least* amount of uranium attenuation over longer time and distance scales. Thus, when the parameter values of Table 9 were used for the downgradient transport predictions discussed in the next section, they provided the least amount of predicted attenuation that was considered to be consistent with the push-pull test data.

The model parameter values were somewhat dependent on the kinetic parameters assumed during the injections into each well, which effectively controlled the unknown (and unverifiable) location of the uranium after injection. If parameters were used that allowed the uranium to move further into the aquifer during injection, then smaller ratios of adsorption to desorption rate constants (i.e., smaller effective partition coefficients, or K_d values) were needed for the adsorption sites to match the observed uranium recovery curves. However, there was a limit to

how far the uranium could be allowed to move into the aquifer before even the extreme assumption of no reaction at all during pumping was insufficient to match the early observed behavior of the uranium. Unfortunately, the site abundance for the slowest adsorption site, which was one of the most important parameters for predicting the downgradient transport of uranium, was quite sensitive to how far the uranium was allowed to move into the aquifer because a higher site abundance was needed if the penetration distance was lower (the same amount of uranium had to be more strongly retained in less aquifer volume, which required a larger site abundance). For this reason, the uranium was allowed to move into the aquifer as far as possible before the matches to the early return concentrations of the uranium were significantly compromised. However, this was a rather subjective process that would benefit from formal model sensitivity tools that were not applied here.

One of the constraints placed on the model parameters was that the ratio of adsorption to desorption rate constants for the fastest and most abundant adsorption site during pumping was fixed to be 0.25 ml/g, which was the maximum deduced ratio from laboratory column experiments that were conducted using downgradient Smith Ranch Highland core material (from MU-3) in a separate study. A tritiated water and uranium breakthrough curve from one of these column experiments, conducted using MP-423 water for the injection, is shown in Fig. 28. The delay in the breakthrough of uranium relative to that of the nonreactive tritiated water, coupled with the known porosity in the column, yielded a ratio of adsorption to desorption rate constant of 0.25 ml/g, which was considered to be an upper bound for the field experiments given the high alkalinity of the MP-423 water compared to the alkalinities that were observed during pumping in the push-pull tests.

One of the troublesome aspects of the adsorption-desorption parameters listed in Table 9 is that the site abundance of the slowest site is quite variable, and it is by far the lowest for the push-pull test conducted with the 4P-61 water (7P-29), which was the injection water that had the lowest uranium concentration (by a factor of more than eight). A lower site abundance for the slowest site was allowable in this case because of the much lower uranium injection concentrations coupled with the observation that the recovery of the injected uranium was similar to that in the other push-pull tests. If the same site abundance had been used in the model as in the 7P-30 test, which had the next lowest site abundance, hardly any uranium would have been predicted to have been recovered in the 7P-29 test. Likewise, the use of the same site abundance providing a good match to the 7P-129 test would have yielded an underprediction of the uranium recovery in the 7P-30 test.

The low site abundance for the 7P-29 test might be partly explained by the fact that 7P-29 was in an area of the ore zone served by HH 7-5 that had an unusually large amount of estimated uranium mineralization in place based on geophysical logs, with nearly 3 times as much uranium ‘under pattern’ as for 7P-129 or 7P-30, and even more of an excess of uranium in the immediate vicinity of the injection well (personal communication from James Clay, Cameco Resources). This large amount of uranium near 7P-29 could have resulted in more of the ‘very strong’ adsorption sites being already occupied by uranium, which would have suppressed the apparent abundance of these sites near this well. However, these same arguments cannot be made for the larger deduced strong site abundance near 7P-129 relative to 7P-30 because 7P-129 had slightly more estimated uranium under pattern than 7P-30. The larger site abundance for 7P-129 relative to 7P-30 is more likely attributable to the fact that the aquifer volume interrogated in the 7P-129 test was much less than in the 7P-30 test, so to predict a similar recovery of injected uranium in both tests (as observed), it was necessary to have a greater site abundance near 7P-129 in the

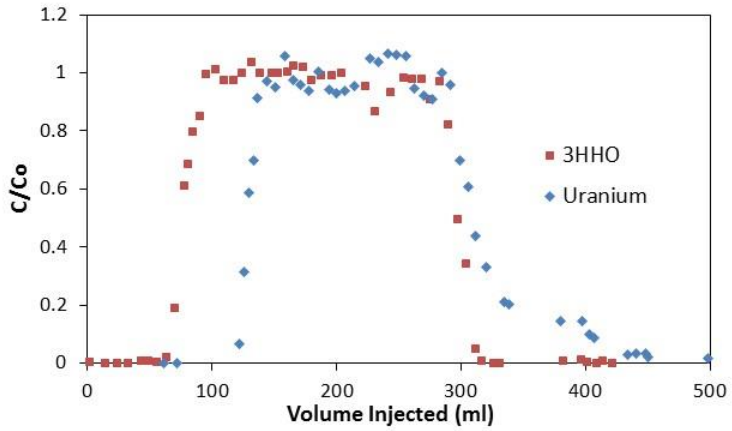

Figure 28. Tritiated water and uranium breakthrough curves in laboratory column experiment involving injection of MP-423 water (spiked with ^{3}HHO) followed by flush of uranium-free water with same pH and alkalinity as MP-423 water. Column was packed with downgradient core material from Smith Ranch-Highland mining unit 3.

model. It is also noteworthy that the water pumped from 7P-129 had by far the lowest ORP values of the three wells, so it is possible that some of the uranium attenuation attributed to adsorption-desorption processes may have actually been caused by reduction in this well (thus leading to a higher apparent abundance of strong adsorption sites).

The preceding discussion clearly points to significant uncertainties in deducing uranium attenuation parameters from the push-pull tests. The model interpretations of the tests would certainly benefit the use of tools that would allow for a rigorous analysis of model sensitivity and uncertainty. They may also benefit from the incorporation of more mechanistic geochemical representations of the attenuation processes (although there may be some question as to whether enough information exists to justify and support such representations). However, there is undoubtedly also significant variability and uncertainty in the hydrogeochemistry in the vicinity of each of the test wells, in the volumes of aquifer interrogated in each test, and in the spatial distributions of tracers and uranium within the aquifer after each injection (especially considering the 'gas lock' hypothesis discussed earlier). Thus, the variability in the deduced model parameters in the three tests may partly reflect real variability in the hydrological and geochemical conditions in the natural system as well as variability in the test conditions. There is also uncertainty associated with how well the unmined ore zone represents the downgradient aquifer.

Predictions of Downgradient Uranium Transport based on Field Test Results

The ultimate objective of this study was to evaluate the ability of the aquifer downgradient of ISR-mined uranium ore zones to attenuate the transport of uranium and other potential problem constituents. To meet this objective, predictive model simulations were conducted of downgradient transport that made use of the field data generated in the study. As previously mentioned, the field data from the push-pull tests did not support evaluations of the attenuation of any potential problem constituents other than uranium because the other constituents of concern (e.g., Se and As) were clearly liberated from the ore zones during the tests, resulting in observed

concentrations of these constituents that were considerably higher than their injection or background concentrations. Thus, the predictive simulations presented here are limited to uranium.

A 1-D numerical model very similar to the model used to estimate uranium adsorption and desorption parameters in the push-pull tests was used to predict uranium transport over much longer time and distance scales downgradient of an ore zone. The model differed only in that it did not simulate radial flow, but rather flow that was 'linear', or of constant velocity as a function of distance in the direction of flow. In the simulations, it was assumed that the downgradient distance to the observation point (where the breakthrough curves were recorded) was the same as the distance across the ore zone, which is approximately true of the distance from the edge of the ore zone to the monitoring well ring at Smith Ranch-Highland in places where ore zones are relatively wide (or if one assumes considerable 'flare' of mining solutions out of narrower ore zones). Under these assumptions, the 'pulse' of water having elevated uranium concentrations from the post-mined ore zone entering the downgradient aquifer will be approximately as long as the travel time from the edge of the ore zone to the monitoring well ring (assuming that the water in the ore zone is displaced with upgradient water that has very low uranium concentrations and the ore zone does not 'bleed' uranium into this upgradient water). It was further assumed that the pulse of uranium from the ore zone migrated through the downgradient aquifer with longitudinal dispersion that corresponded to a Peclet number of 8, the Peclet number deduced from the two cross-well tests conducted in this study.

Given all these assumptions, the breakthrough curves of both a nonreactive species and uranium at the monitoring well ring, using the uranium adsorption and desorption parameters of Table 9 (corresponding to each of the push-pull tests) are shown in Figs. 29 to 31, respectively. The dashed lines in these figures show the breakthrough curves predicted under the same set of conditions with a Peclet number of 100, corresponding to much less flow dispersion (much closer to piston flow), in the downgradient aquifer. Note that the x axis in these figures is pore volumes, not time, where a pore volume is defined as the volume of the downgradient aquifer between the ore zone and the monitoring well ring (this is also the pore volume of the ore zone under the assumptions given above). It is apparent that when the flow dispersion deduced from the two cross-well tracer tests in MU-4 is used in the simulations there is an earlier arrival of uranium at the monitoring well ring than if little dispersion is assumed. However, the peak concentrations of uranium at the monitoring ring are lower when more dispersion is assumed, so the early arrival is counter-balanced by the decrease in peak concentrations.

The uranium concentration in the ore zone in each simulation of Figs. 29 to 31 was assumed to be the same as the injection concentration in the corresponding push-pull test from which the adsorption/desorption parameters were estimated. In the case of Figs. 29 and 30, which correspond to the 7P-129 and 7P-30 tests, these uranium concentrations are ~40 mg/L, which is much higher than one would normally expect from a 'restored' ore zone. However, if the concentrations were reduced to ~5 mg/L, matching the 'partially-restored' water used in the 7P-29 test, the peak simulated concentrations at the monitoring well ring would be well below background concentrations in Figs. 29 and 30 because of the greater abundance of the slowest/strongest adsorption sites in these simulations. Thus, the simulation of Fig. 31 effectively serves as a worst-case scenario, not only because it has the highest predicted normalized uranium concentrations of any of the three cases, but because the abundance of the strongest sites is at least an order of magnitude less than in the other two simulations (see values for S_{m3} in Table 9).

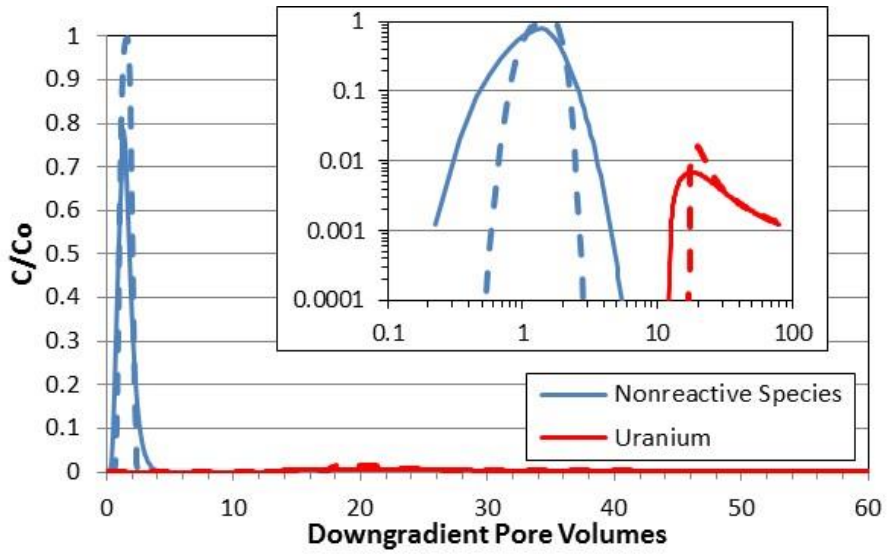

Figure 29. Predictions of downgradient transport of uranium and a nonreactive species using the uranium transport parameters from the 7P-129 push-pull test. Solid lines are Peclet number of 8 and dashed lines are Peclet number of 100. Inset shows log-log axes. Uranium ore zone concentration is assumed to be ~40 mg/L, and the ore zone is assumed to be one pore volume.

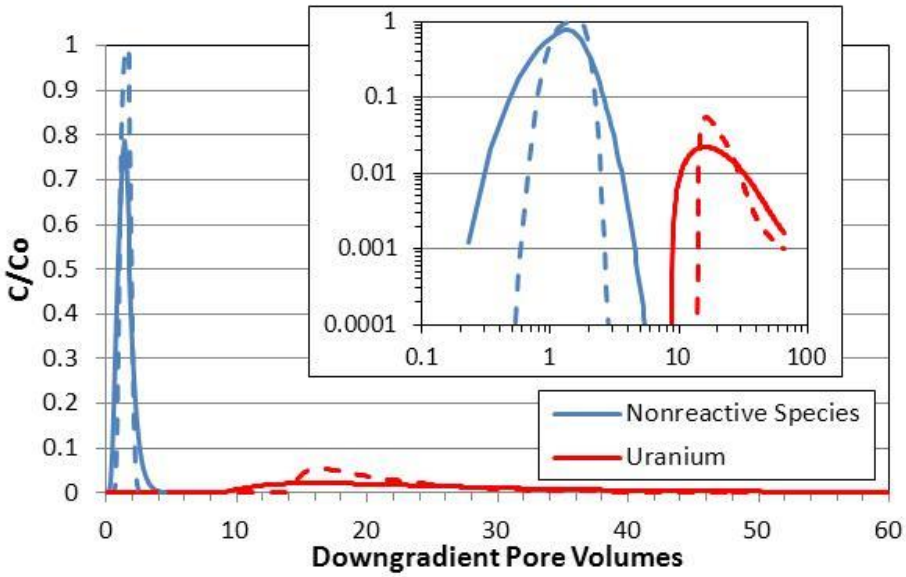

Figure 30. Predictions of downgradient transport of uranium and a nonreactive species using the uranium transport parameters from the 7P-30 push-pull test. Solid lines are Peclet number of 8 and dashed lines are Peclet number of 100. Inset shows log-log axes. Uranium ore zone concentration is assumed to be ~40 mg/L, and the ore zone is assumed to be one pore volume.

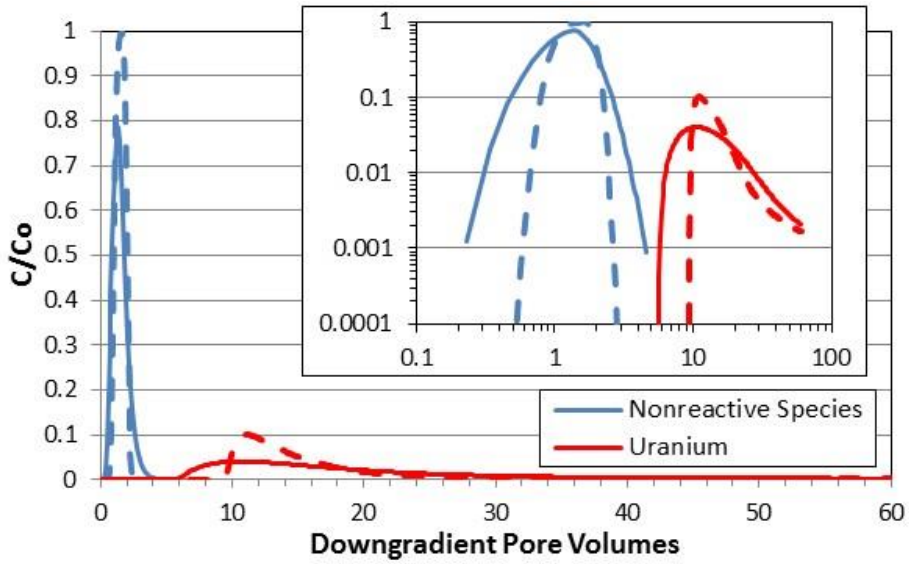

Figure 31. Predictions of downgradient transport of uranium and a nonreactive species using the uranium transport parameters frm the 7P-29 push-pull test. Solid lines are Peclet number of 8 and dashed lines are Peclet number of 100. Inset shows log-log axes. Uranium ore zone concentration is assumed to be ~4.7 mg/L, and the ore zone is assumed to be one pore volume.

It should be pointed out that the predictions of Figs. 29 to 31 are relatively independent of the flow velocity assumed or the travel time required for a nonreactive species to reach the monitoring well ring. If the travel time increases by a factor of 2, then the time that the elevated concentrations from the ore zone will enter the downgradient aquifer will also increase by a factor of 2, and the net result will be almost no difference in the predicted concentrations at the monitoring well ring (they will just take twice as long to rise and fall). There are two reasons for this result: (1) over the time scales anticipated, all three adsorption/desorption reactions/sites behave essentially as if they are at local equilibrium, and (2) the uranium attenuation in all cases is dictated primarily by the abundance of very strong adsorption sites relative to the amount of uranium in the ore zone pulse, which is the same regardless of how long the pulse takes to move downgradient.

Fig. 32 shows the effect of doubling the distance to the monitoring well ring relative to the width of the ore zone when using the adsorption/desorption parameters deduced from the 7P-29 push-pull test (i.e., use Fig. 31 for comparison). It is apparent that the concentrations at the observation point are significantly lowered, and also delayed in arriving, relative to Fig. 31. This case could also be considered to represent a situation where the compliance boundary is twice as far from the ore zone as the monitoring well ring.

If one assumes that the unrecovered mass of uranium in the push-pull tests was permanently immobilized in the aquifer, then a much simpler way to express the attenuation capacity of the downgradient aquifer from the push-pull test results is to simply divide the mass of unrecovered uranium by the volume of aquifer interrogated. Of course, there is uncertainty in the volume of aquifer interrogated because of the apparent differences in the distribution of flow going out of and coming back into the wellscreens during the tests (discussed above). There is also uncertainty in how far the uranium actually penetrated into the aquifer relative to the nonreactive tracers. However, if it is assumed that the interrogation volume was equal to the

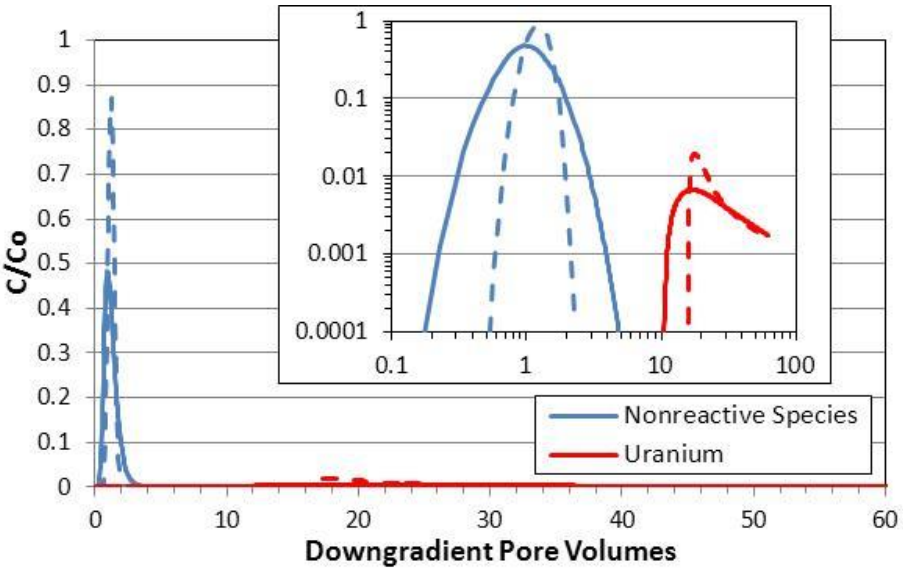

Figure 32. Predictions of downgradient transport of uranium and a nonreactive species using the uranium transport parameters from the 7P-30 push-pull test and assuming that the downgradient distance is twice that of the ore zone width (ore zone is half a pore volume). Solid lines are Peclet number of 8 and dashed lines are Peclet number of 100. Inset shows log-log axes. Uranium ore zone concentration is assumed to be ~40 mg/L.

volume of injected water plus chase water (likely an underestimate from the standpoint of the flow distribution differences but an overestimate from the standpoint of how far the uranium was likely to have penetrated), then the uranium 'immobilized' per unit volume of aquifer was 2.85 g/m^3 in the 7P-129 test, 4.06 g/m^3 in the 7P-30 test, and 0.38 g/m^3 in the 7P-29 test. These estimates assume a flow porosity of 0.25 in the aquifer. The 7P-29 test yields by far the smallest apparent immobilization capacity because the injection concentration of uranium was about 8 times lower in this test than in the other tests, but the fraction of injected uranium recovered was similar to the other tests.

Discussion and Conclusions

The results of the predictive modeling in the previous section indicate that, based on the information obtained from the cross-well and push-pull field tests, the aquifer downgradient of an ISR-mined ore zone should be capable of significantly attenuating the transport of uranium. The predictions suggest that it might be possible to relax conservatism in ore zone restoration targets and in post-restoration monitoring requirements while still ensuring the safety of the environment and public. These results are particularly encouraging considering that most assumptions made in both the interpretive and predictive modeling efforts were pessimistic from the standpoint of maximizing the predicted rate and amount of uranium transport. For example, the abundance of very strong adsorption sites was minimized, the desorption rate constants for these sites were maximized, and it was assumed that there was no irreversible immobilization of uranium (e.g., reduction). If any of these pessimistic assumptions are relaxed, the uranium attenuation will only be predicted to be greater than in the predictions of the previous section.

Also, it is important to keep in mind that the uranium injection concentrations in two of the three push-pull tests (~40 mg/L) greatly exceeded what would be expected from a 'restored' post-mined ore zone because these waters had not been subjected to any restoration. The use of these waters could be argued to have provided a pessimistic interrogation of the unmined ore zone. However, a counter-argument to this claim is that the push-pull test in which a 'partially-restored' water was injected showed no greater fraction of uranium attenuated than the tests using the unrestored waters.

Despite the encouraging results of this study, many uncertainties and questions remain. Most of these have been discussed in previous sections of this report. The issue of how representative two five-spot patterns and three push-pull tests can be for an entire downgradient aquifer is a fair question that will undoubtedly be raised, especially since the tests were conducted in ore zones, not downgradient aquifers. However, the field tests certainly interrogated much more aquifer volume and heterogeneity than any laboratory tests ever could, and they did so while minimizing the disturbance of ambient aquifer conditions.

To reduce uncertainties, it is suggested that a cross-well test involving the injection of a post-mined ore zone water into an injection well while a nearby production well is being pumped be considered in an unmined ore zone. Such a test would interrogate much more aquifer volume and heterogeneity than a single-well push-pull test. Also, nonidealities/artifacts such as altered geochemical conditions near wellbores (e.g., high pH from grout in well completions) and gas-locking or other flow restrictions during injection would have much less influence on test results and interpretations than in a single-well test. However, based on the results of this study, a large volume of previously-mined ore zone water (and unrestored at that) would have to be injected to expect to be able to see any uranium in a nearby production well, and this might pose logistical challenges.

It would be better to conduct such a cross-well test in a downgradient aquifer instead of an unmined ore zone, but this would require installation of additional wells and pose environmental permitting challenges in addition to the same logistical challenges of an ore zone test. It is suggested that consideration be given to installing additional downgradient wells into wellfields when they are being designed and constructed (with the monitoring well ring expanded to accommodate these wells) so that downgradient testing might be easily incorporated into a site-specific restoration and stability strategy. It is possible that such wells could be used as pumping wells to simply draw water toward them from the post-mined ore zone, thus avoiding the logistical difficulties of having to inject water anywhere. In this case it would be advisable to introduce a nonreactive tracer into the ore zone during the mining process so that the arrival of waters from the ore zone could be identified independently of the arrival of uranium and other contaminants at the downgradient wells. At Smith Ranch-Highland, the chloride introduced from ion exchange resins serves this purpose because of the very low background concentrations of chloride in the groundwater.

Acknowledgments

Most of the funding for this work was provided by the University of Wyoming, School of Energy Resources, which administered funds appropriated by the Wyoming State Legislature for research activities related to uranium ISR in Wyoming. Partial funding for the push-pull tests was also provided by the U.S. Environmental Protection Agency Regional Applied Research Effort (RARE) program. The authors are grateful to many people at Cameco Resources for providing

access to the Smith Ranch-Highland ISR site and for their logistical and technical support of the field tests, as well as their perseverance in pursuing environmental approvals for the tests. We especially thank Brent Berg, Larry Reimann, Ken Garoutte, Brett Henderson, Craig Hiser, Mike Beshore, Dennis Zimbelman and the analytical laboratory staff of Cameco.

References

Davis, J.A., Curtis, G.P., 2003. Application of Surface Complexation Modeling to Describe Uranium(VI) Adsorption and Retardation at the Uranium Mill Tailings Site at Naturita, Colorado, *NUREG/CR-6820*, United States Geological Survey (for Nuclear Regulatory Commission), Menlo Park, CA.

Dittrich, T.M. and P. W. Reimus. 2015. Uranium transport in a crushed granodiorite: Experiments and reactive transport modeling, *J. Contaminant Hydrology*, 175-176, 44-59.

Dong, W., Brooks, S., 2006. Determination of the formation constants of ternary complexes of uranyl and carbonate with alkaline earth metals (Mg^{2+}, Ca^{2+}, Sr^{2+}, and Ba^{2+}) using anion exchange method. *Env. Sci. Tech.*, 40(15), pp. 4689–4695.

Johnson, J., 2010. llnl.dat 4023 2010-02-09. Data from 'thermo.com.V8.R6.230' prepared by Jim Johnson at Lawrence Livermore National Laboratory, in Geochemist's Workbench format. Converted to PHREEQC format by Greg Anderson with help from David Parkhurst.

Lake, L. 1989. *Enhanced Oil Recovery*. Prentice Hall, Englewood Cliffs, NJ.

Norwest Corporation. 2013. *Mine Unit 7 Hydrologic Test Report*. Prepared for Cameco Resources Smith Ranch-Highland Uranium Project.

Parkhurst, D. L., Appelo, C. A. J., 2013. PHREEQC (Version 3.0.4) - A computer program for speciation, batch speciation, one-dimensional transport, and inverse geochemical calculations, U.S. Geological Survey Techniques and Methods, Book 6, Chapter A43, p. 497, http://pubs.usgs.gov/tm/06/a43/.

Pelizza, M. S. 2008. In-Situ Recovery of Uranium, *Southwest Hydrology*, 7(6), p. 28 (http://www.swhydro.arizona.edu/archive/V7_N6/feature6.pdf).

Reimus, P. W., Pohll, G., Mihevc, T., Chapman, J. Papelis, L., Lyles, B., Kosinski, S., Niswonger, R., and Sanders, P. 2003. "Testing and Parameterizing a Conceptual Model for Radionuclide Transport in a Fractured Granite using Multiple Tracers in a Forced-Gradient Test", *Water Resources Res.*, 39(12), 1350, doi:10.1029/2002WR001597.

Richter, S., Alonso-Munoz, A., Eykens, R., Jacobsson, U., Kuehn, H., Verbruggen, A., Aregbe, Y., Wellum, R., and Keegan, E. 2008. The isotopic composition of natural uranium samples - Measurements using the new n(U-233)/n(U-236) double spike IRMM-3636. *Int J Mass Spectrom* **269**, 145-148.

Stirling, C. H., Andersen, M. B., and Warthmann, R. 2015. Isotope fractionation of 238 U and 235 U during biologically-mediated uranium reduction, *Geochimica et Cosmochimica Acta*, 163:200-218.

Stylo, M., Neubert, N., Wang, Y., Monga, N., Romaniello, S. J., Weyer, S., and Bernier-Latmani, R. 2015. Uranium isotopes fingerprint biotic reduction, *Proceedings of the National Academy of Sciences, USA*, 112(18):5619-5624.

World Nuclear Association. 2014. In-Situ Leach (ISL) Mining of Uranium, http://www.world-nuclear.org/info/Nuclear-Fuel-Cycle/Mining-of-Uranium/In-Situ-Leach-Mining-of-Uranium.

Appendix A: Photographs from Cross-Well Tracer Tests

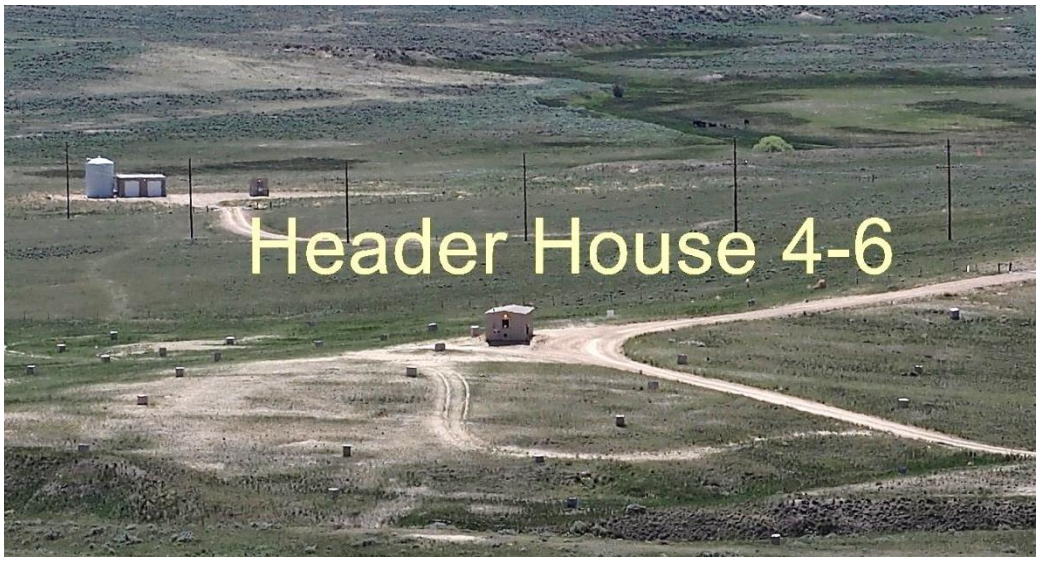

Figure A-1. View of Header House 4-6 looking toward the west from near the middle of MU-4.

Figure A-2. Close up view of Header House 4-6.

Figure A-3. View inside Header House 4-6 during cross-well tracer test.

Figure A-4. Close-up view of circulation loop plumbing for 4P-121 well pattern.

Figure A-5. Mixing concentrated tracer solutions in carboys.

Figure A-6. Garbage bins used for dispensing concentrated tracer solution, and high-pressure peristaltic pumps (red) used to inject tracer into circulating injection flows. Autosampler is inside of blue bin on shelf; peristaltic pump feeding autosampler is to right of bin.

Figure A-7. Close-up view of autosampler loaded with sample bottles inside bin.

Appendix B: Photographs from Single-Well Push-Pull Tests

Figure B-1. Header House 7-5, October 2014.

Figure B-2. Header House 7-5, January 2015.

Figure B-3. Measuring field parameters with YSI sonde/meter and Hach kits while tank truck is being filled with 4P-61water.

Figure B-4. Purging tank truck headspace with $CO_2/H_2/N_2$ gas mixture at MP-423.

Figure B-5. Injecting MP-423 water into 7P-30 at Header House 7-5.

Figure B-6. YSI sonde and meter with flow cell inside HH 7-5. Cooler top was used for alkalinity measurements and Hach reagent kit measurements of Fe^{2+} and S^{2-}.

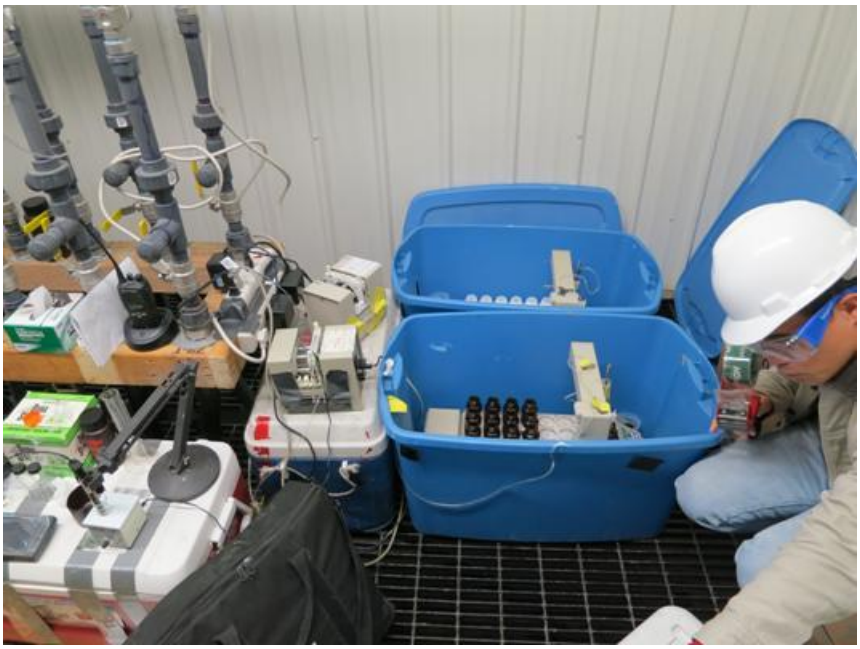

Figure B-7. Dual autosampler setup in HH 7-5 to collect samples for tracer analyses and also for uranium and general chemistry analyses.

Figure B-8. Plumbing on production wellhead to divert flow to autosamplers and YSI flow cell. Sample collection point for filtered grab samples for uranium isotope analyses is shown.

Appendix C: Additional Plots of Results from Single-Well Push-Pull Tests

Results for 7P-129

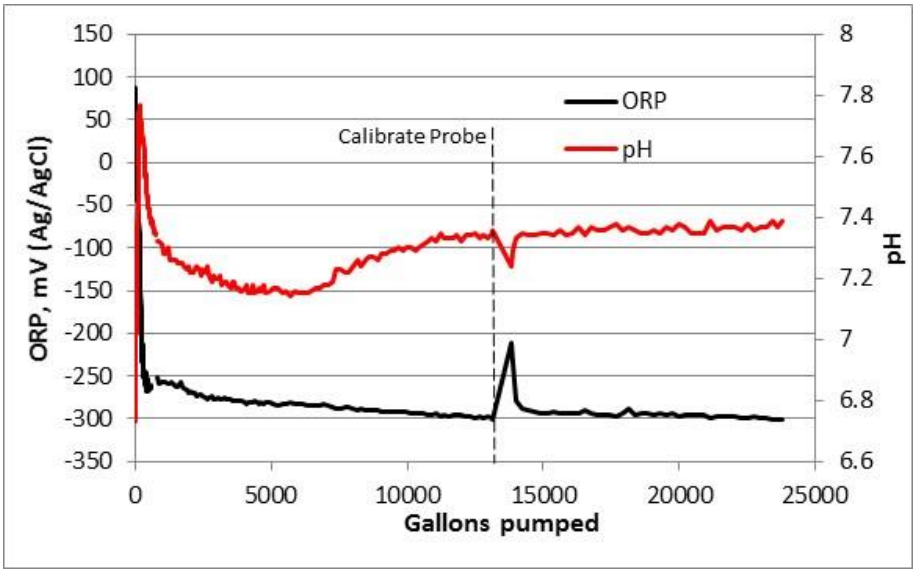

Figure C-1. ORP and pH during pumping of 7P-129.

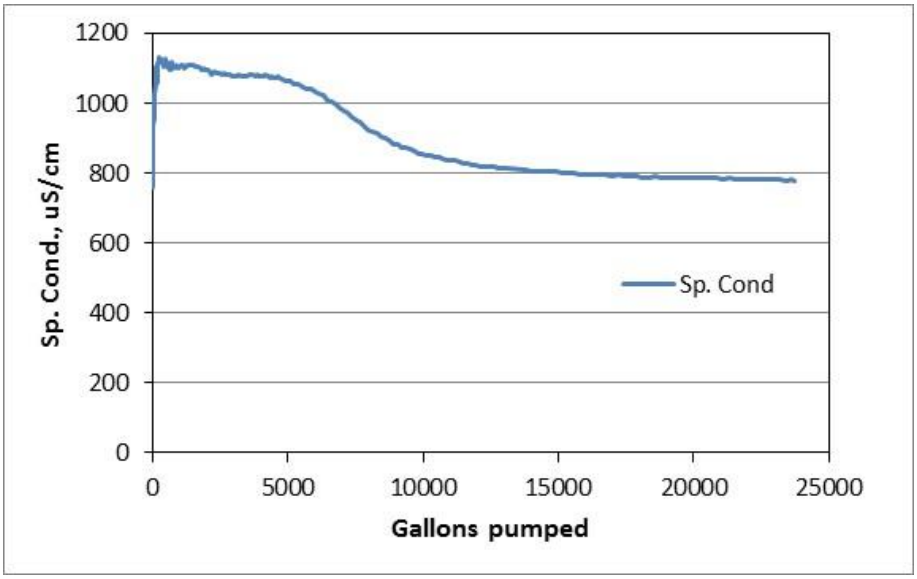

Figure C-2. Specific conductance during pumping of 7P-129.

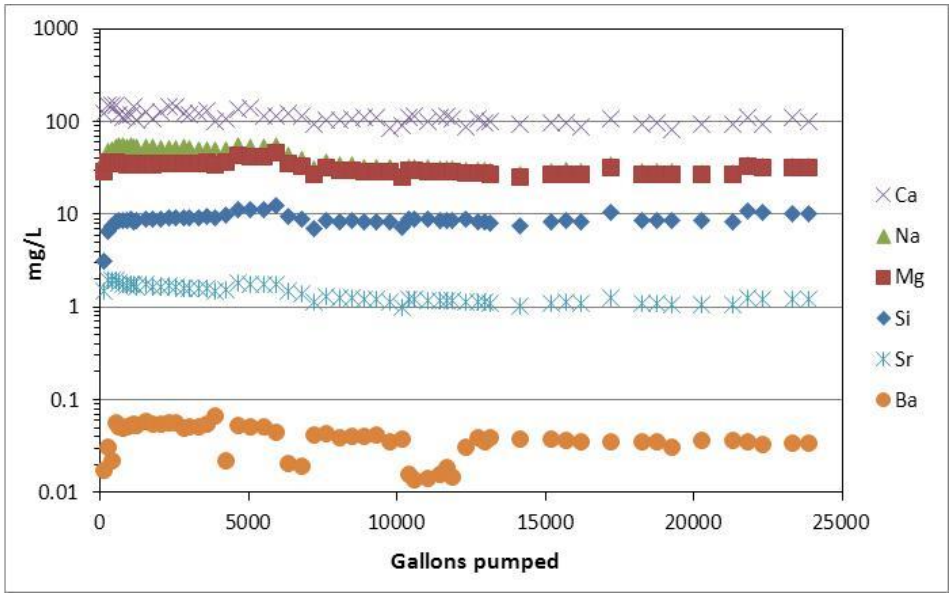

Figure C-3. Cations measured by ICP-OES during pumping of 7P-129.

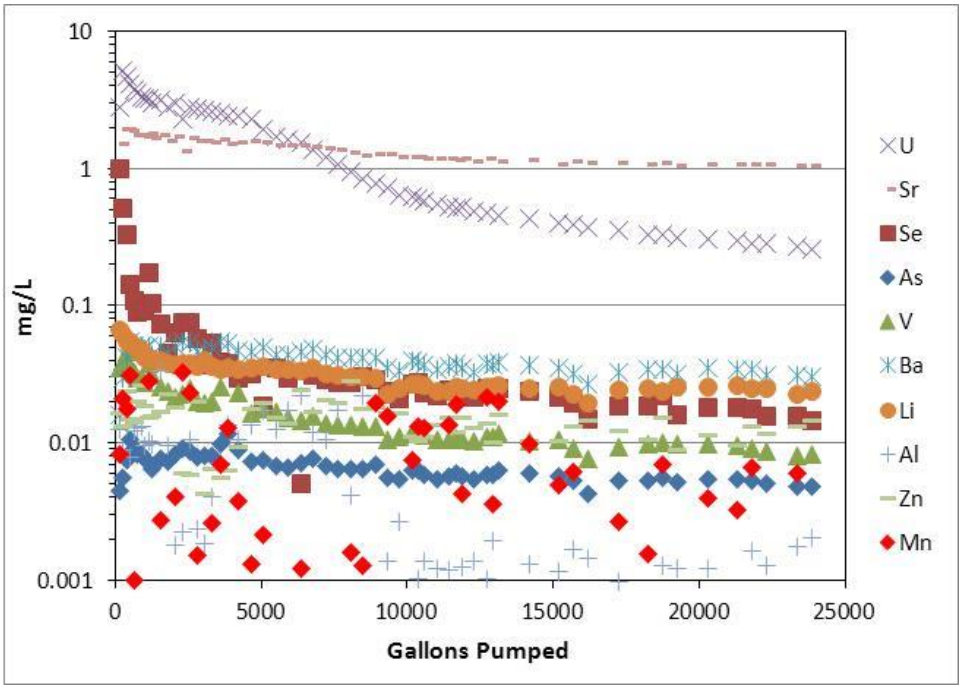

Figure C-4. 'Trace' and minor elements measured by ICP-MS during pumping of 7P-129.

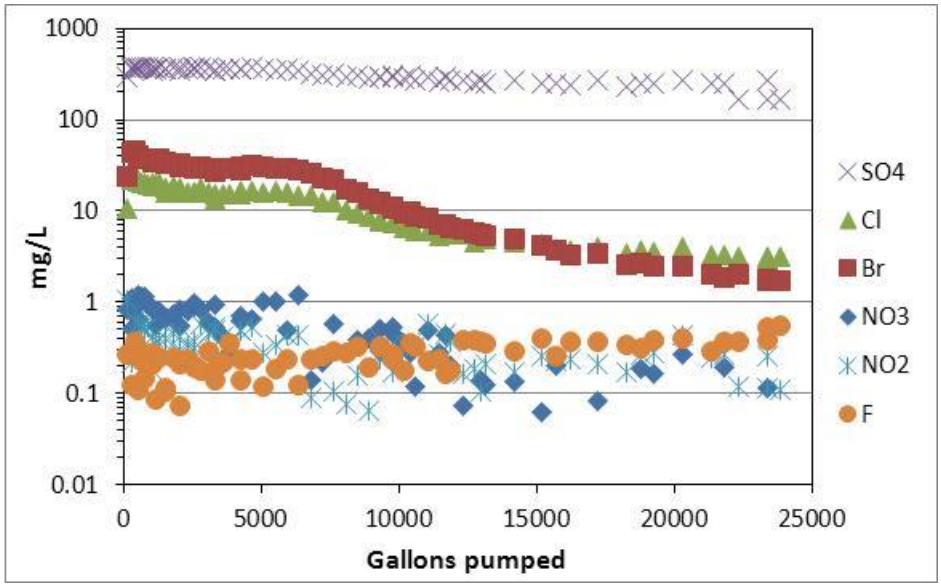

Figure C-5. Anions measured by ion chromatography during pumping of 7P-129.

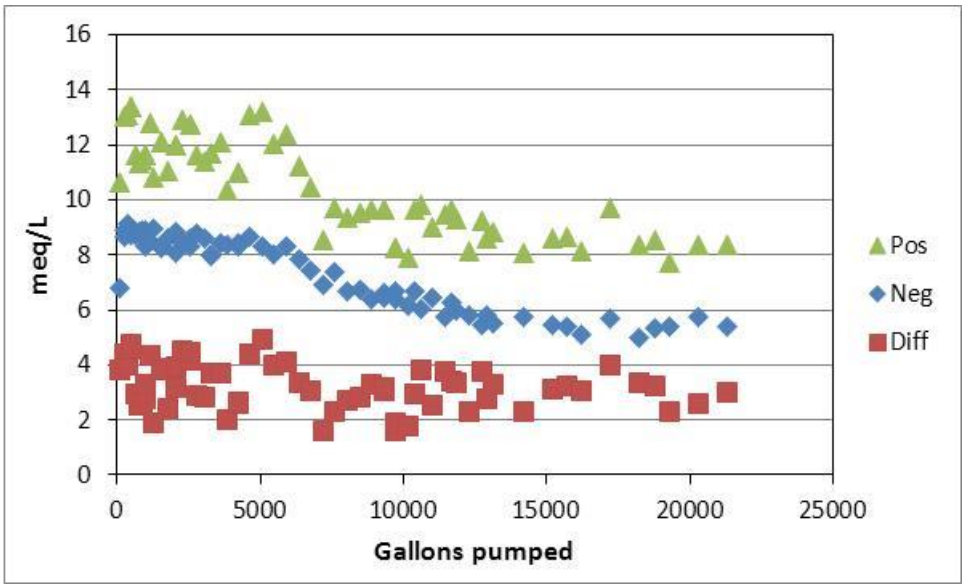

Figure C-6. Positive and negative charge imbalance during pumping of 7P-129. Difference is attributable to HCO_3^-, which is not measured by ion chromatography.

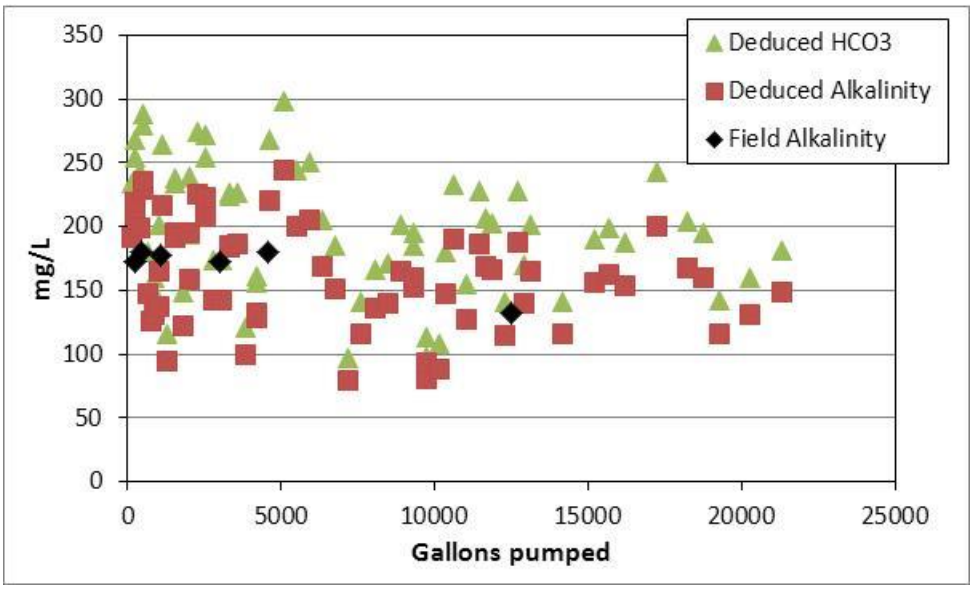

Figure C-7. HCO_3^- deduced from charge imbalance during pumping of 7P-129, and alkalinity (mg/L $CaCO_3$) calculated from HCO_3^- with comparison to field-measured alkalinities.

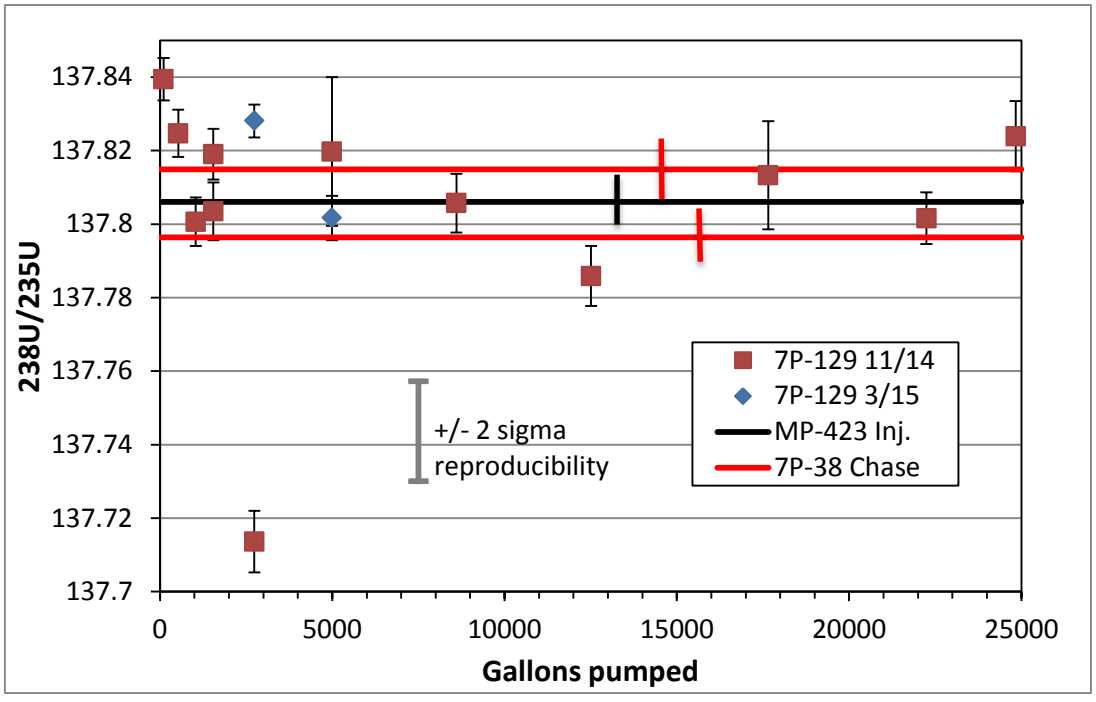

Figure C-8. $^{238}U/^{235}U$ ratios during pumping of 7P-129. Two-sigma reproducibility (two times standard deviation) is for numerous measurements of an external standard (NIST 960). Error bars on individual data points (including MP-423 and 7P-38 lines) are two-sigma values for the individual measurements.

Results for 7P-30

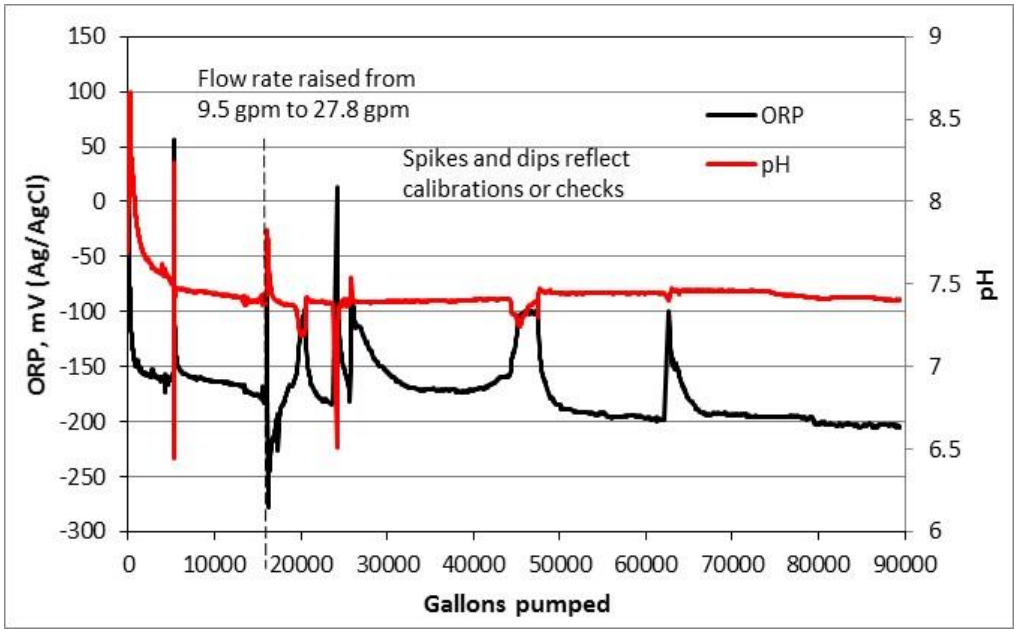

Figure C-9. ORP and pH during pumping of 7P-30.

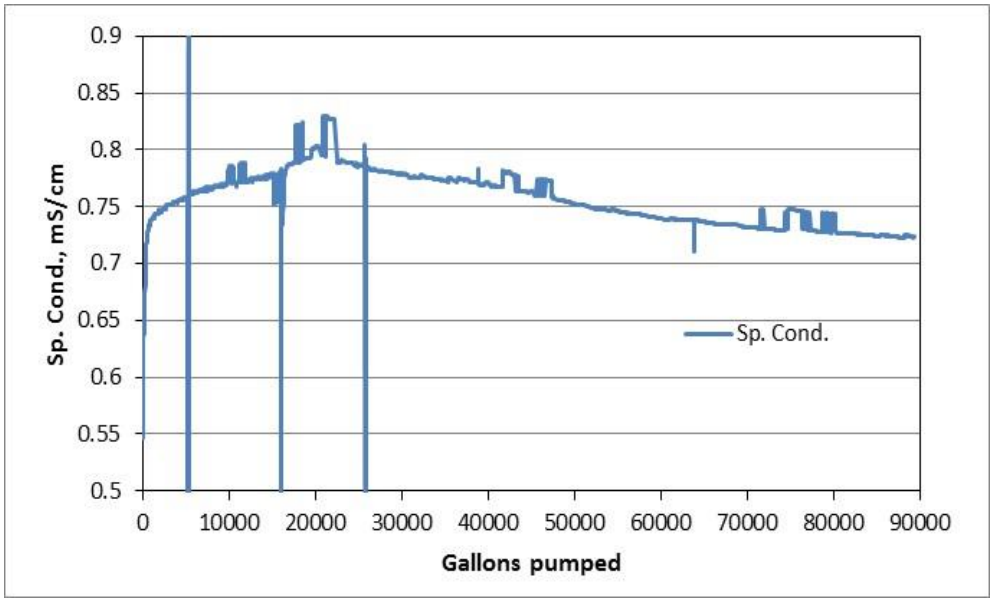

Figure C-10. Specific conductance during pumping of 7P-30.

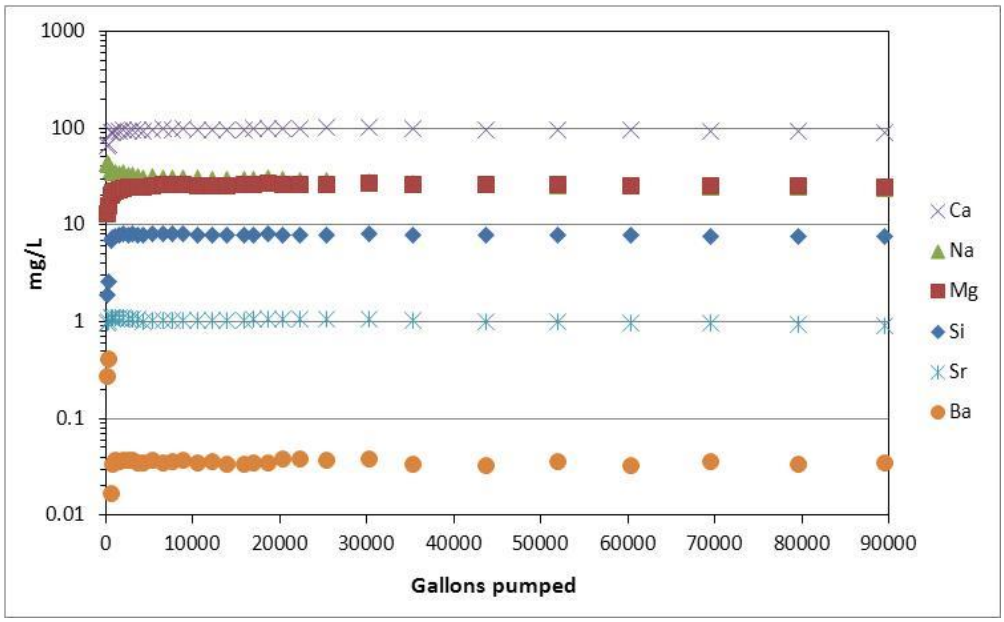

Figure C-11. Cations measured by ICP-OES during pumping of 7P-30.

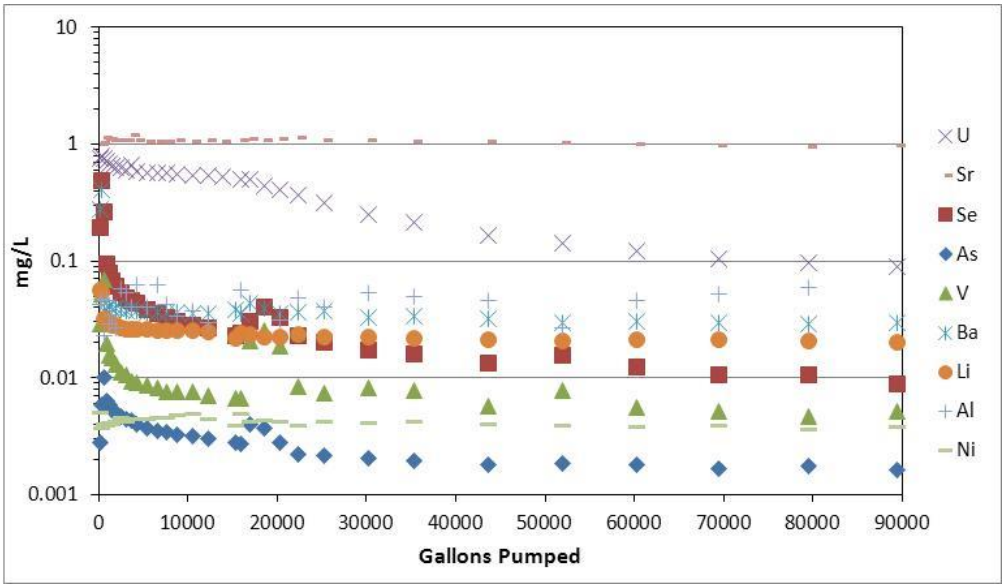

Figure C-12. 'Trace' and minor elements measured by ICP-MS during pumping of 7P-30.

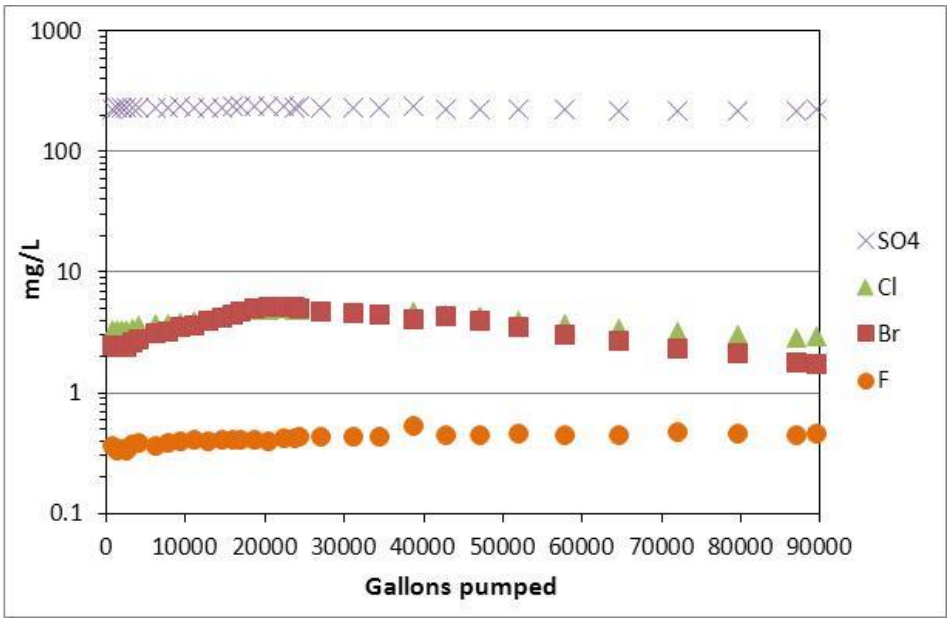

Figure C-13. Anions measured by ion chromatography during pumping of 7P-30.

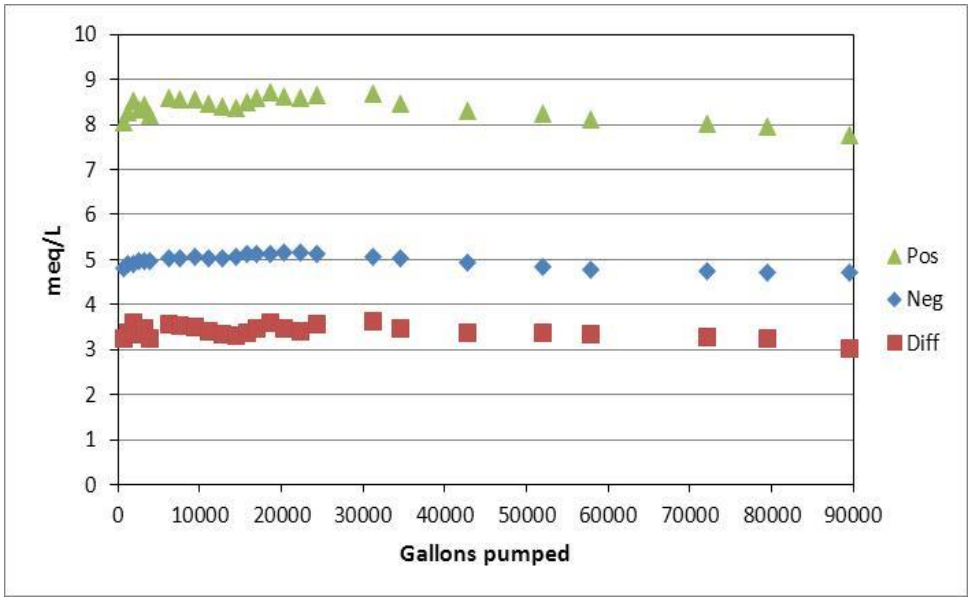

Figure C-14. Positive and negative charge imbalance during pumping of 7P-30. Difference is attributable to HCO_3^-, which is not measured by ion chromatography.

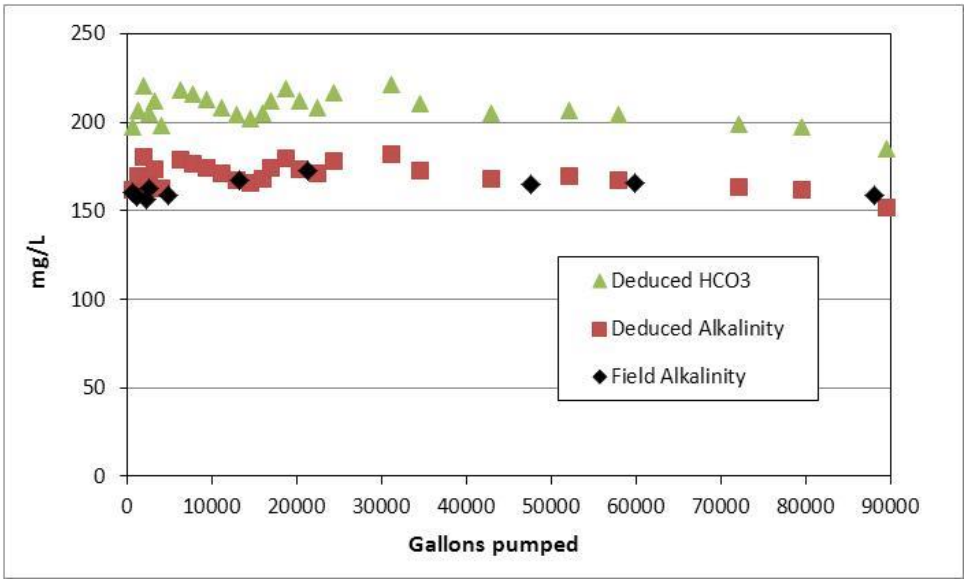

Figure C-15. HCO_3^- deduced from charge imbalance during pumping of 7P-30, and alkalinity (mg/L $CaCO_3$) calculated from HCO_3^- with comparison to field-measured alkalinities.

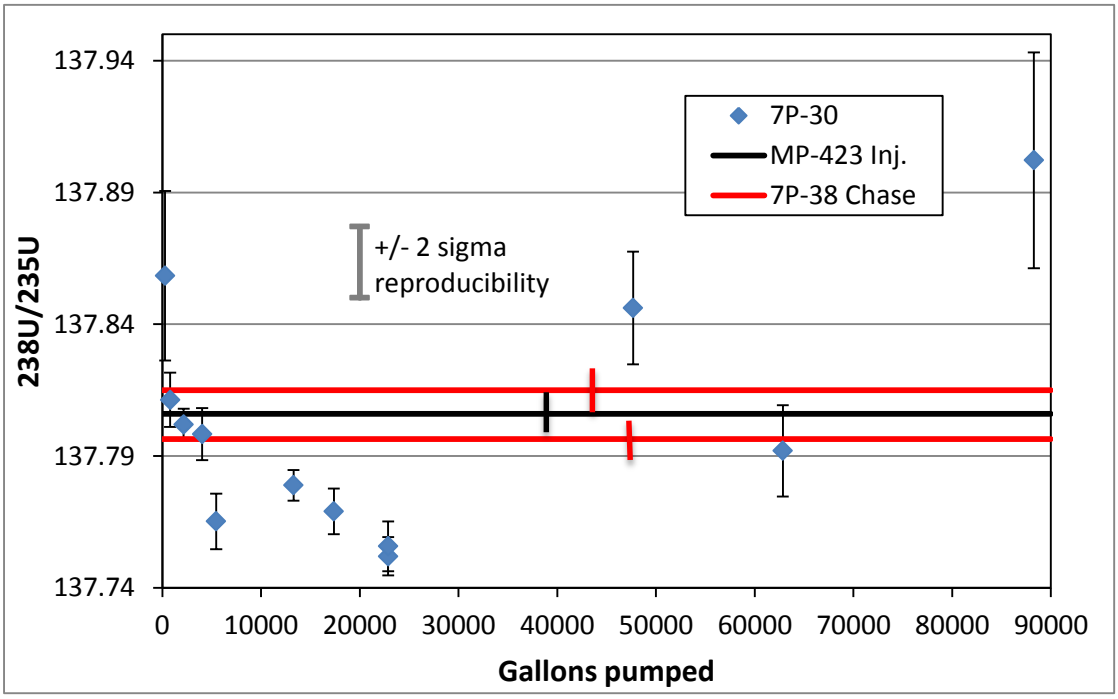

Figure C-16. $^{238}U/^{235}U$ ratios during pumping of 7P-30. Two-sigma reproducibility (two times standard deviation) is for numerous measurements of an external standard (NIST 960). Error bars on individual data points (including MP-423 and 7P-38 lines) are two-sigma values for the individual measurements.

Results from 7P-29

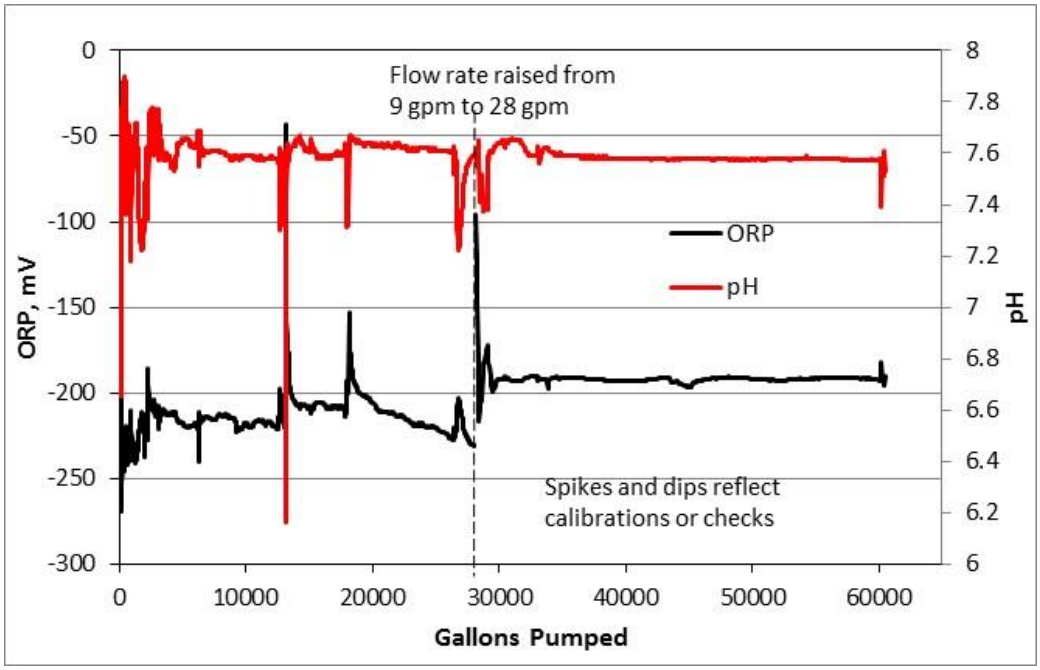

Figure C-17. ORP and pH during pumping of 7P-29.

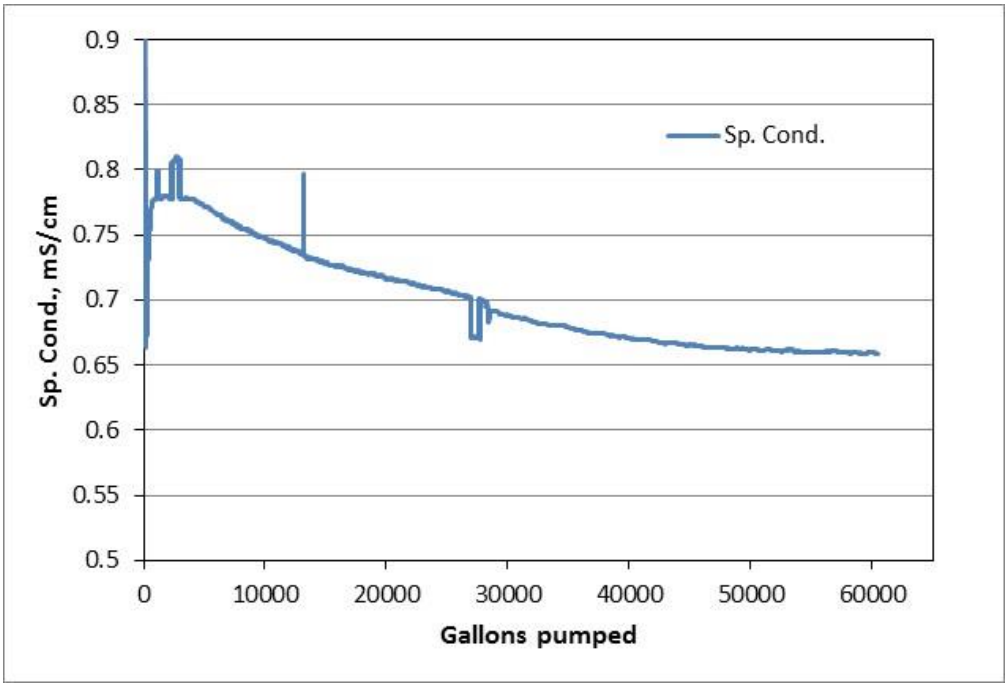

Figure C-18. Specific conductance during pumping of 7P-29.

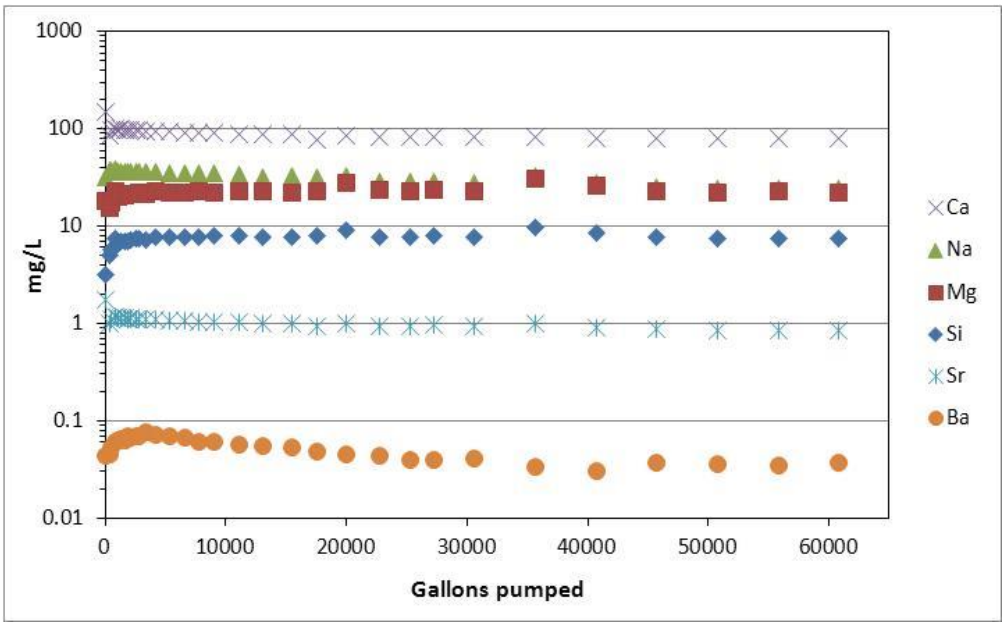

Figure C-19. Cations measured by ICP-OES during pumping of 7P-29.

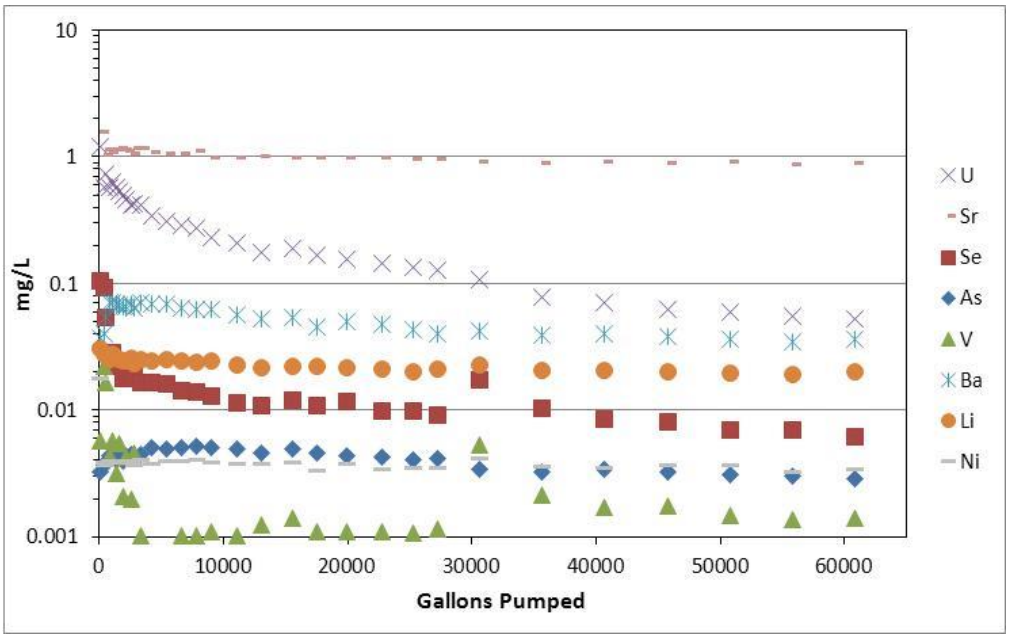

Figure C-20. 'Trace' and minor elements measured by ICP-MS during pumping of 7P-29.

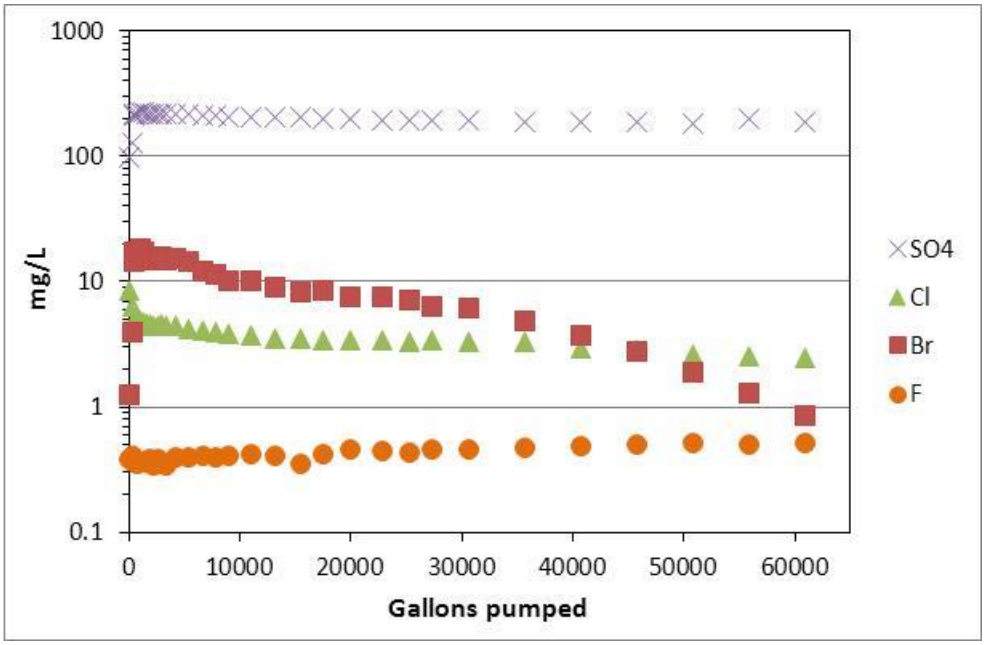

Figure C-21. Anions measured by ion chromatography during pumping of 7P-29.

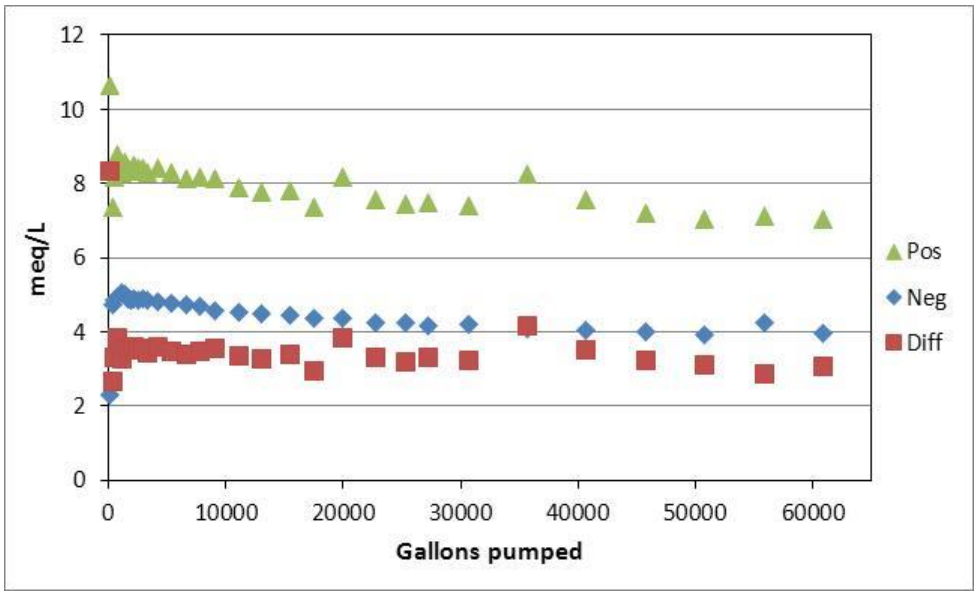

Figure C-22. Positive and negative charge imbalance during pumping of 7P-29. Difference is attributable to HCO_3^-, which is not measured by ion chromatography.

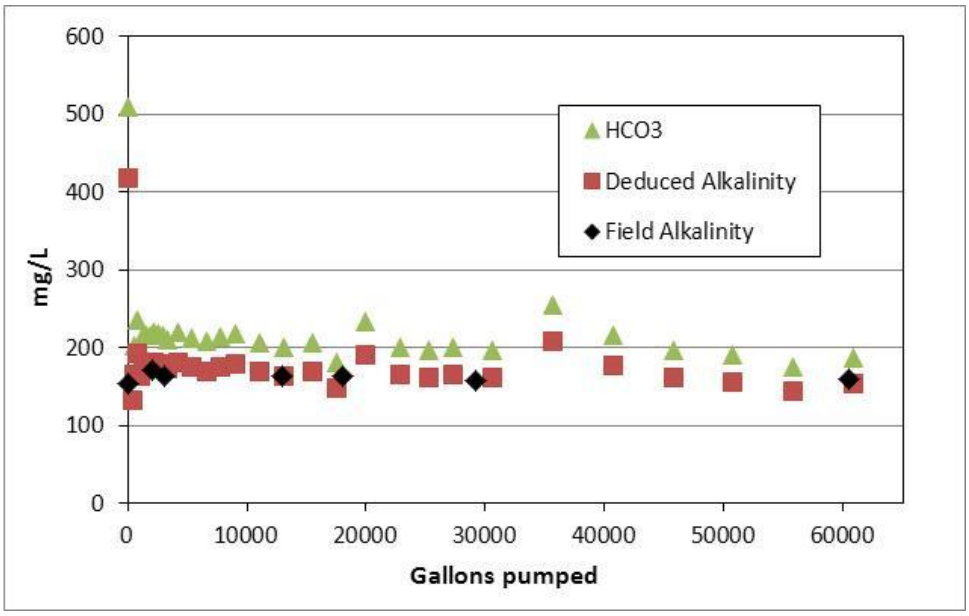

Figure C-23. HCO_3^- deduced from charge imbalance during pumping of 7P-29, and alkalinity (mg/L $CaCO_3$) calculated from HCO_3^- with comparison to field-measured alkalinities.

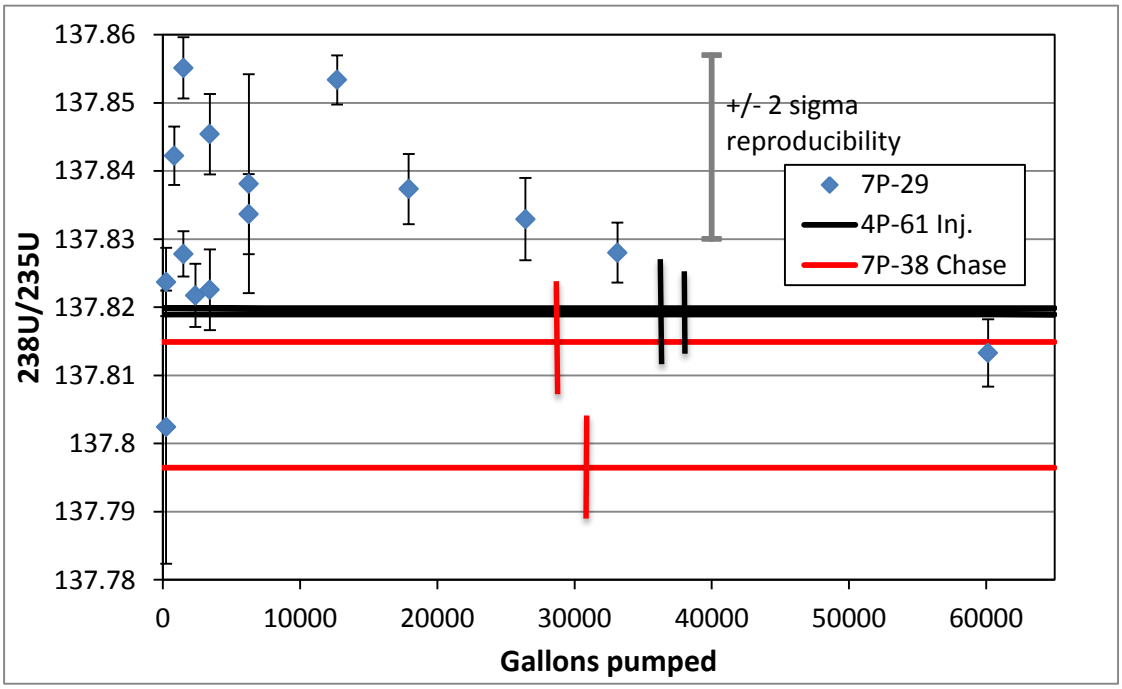

Figure C-24. $^{238}U/^{235}U$ ratios during pumping of 7P-29. Two-sigma reproducibility (two times standard deviation) is for numerous measurements of an external standard (NIST 960). Error bars on individual data points (including 4P-61 and 7P-38 lines) are two-sigma values for the individual measurements.